SEISMIC BEHAVIOR OF AUTOCLAVED AERATED CONCRETE REINFORCED VERTICAL PANEL BUILDINGS

A THESIS SUBMITTED TO
THE GRADUATE SCHOOL OF NATURAL AND APPLIED SCIENCES
OF
MIDDLE EAST TECHNICAL UNIVERSITY

BY

FURKAN GÖKMEN

IN PARTIAL FULFILLMENT OF THE REQUIREMENTS
FOR
THE DEGREE OF MASTER OF SCIENCE
IN
CIVIL ENGINEERING

SEPTEMBER 2017

Approval of the thesis:

SEISMIC BEHAVIOR OF AUTOCLAVED AERATED CONCRETE REINFORCED VERTICAL PANEL BUILDINGS

submitted by **FURKAN GÖKMEN** in partial fulfillment of the requirements for the degree of **Master of Science in Civil Engineering Department, Middle East Technical University** by,

Prof. Dr. Gülbin Dural Ünver
Dean, Graduate School of **Natural and Applied Sciences** _____

Prof. Dr. İsmail Özgür Yaman
Head of Department, **Civil Engineering** _____

Prof. Dr. Barış Binici
Supervisor, **Civil Engineering Dept., METU** _____

Examining Committee Members:

Prof. Dr. Kağan Tuncay
Civil Engineering Dept., METU _____

Prof. Dr. Barış Binici
Civil Engineering Dept., METU _____

Prof. Dr. Altuğ Erberik
Civil Engineering Dept., METU _____

Prof. Dr. Erdem Canbay
Civil Engineering Dept., METU _____

Assoc. Prof. Dr. Ramazan Özçelik
Civil Engineering Dept., Akdeniz University _____

Date: _____

I hereby declare that all information in this document has been obtained and presented in accordance with academic rules and ethical conduct. I also declare that, as required by these rules and conduct, I have fully cited and referenced all material and results that are not original to this work.

Name, Last name: Furkan Gökmen

Signature :

ABSTRACT

SEISMIC BEHAVIOR OF AUTOCLAVED AERATED CONCRETE REINFORCED VERTICAL PANEL BUILDINGS

Gökmen, Furkan

M.S., Department of Civil Engineering

Supervisor: Prof. Dr. Barış Binici

September 2017, 76 pages

In this study, the seismic behavior of Autoclaved Aerated Concrete (AAC) reinforced panel walls and buildings was investigated. The structural members were investigated under cyclic lateral loading and axial load and the results were compared with the previous tests. The main objective of this study was to provide recommendations for nonlinear analysis of the reinforced AAC panel walls and buildings. OpenSees platform was chosen as the computational platform. The walls were modeled with fiber sections. The fiber sections were composed of AAC and steel reinforcement fibers. The reinforcement was modeled with hysteretic material to provide the cyclic behavior. These fiber sections were used in nonlinear force based beam-column frame elements in order to investigate the nonlinear behavior. Then, the panel walls previously tested at METU were simulated by controlling displacements method under increasing cyclic deformations. Axial load ratio (N/N_0) was found to affect the model response; therefore, two sets of modeling parameters were proposed for cases less than and more

than 10% of wall axial load carrying capacity. Using three plus one panel results, the four-panel wall models were found to satisfactorily estimate the multi-panel response.

The full-scale building test was also modeled by using groups of maximum three panels. Static and incremental dynamic analyses were conducted to match the experimental results of the building. Afterward, an incremental dynamic analysis was conducted to observe the relationship between ground motion scale factor and maximum interstory drift ratio.

The key outcomes from this thesis are; i) AAC buildings, due to their lightweight nature, are expected to behave in their pre-yielding regions under design earthquakes, ii) under extreme events, there seems to exist some deformation and energy dissipation capacity which can help AAC buildings to swing without collapse. Based on these results AAC buildings appear to be a good alternative for low rise construction in seismic regions.

Keywords: Autoclaved Aerated Concrete, AAC, Vertical Reinforced AAC Panels, Reinforced Panel Buildings, Nonlinear Analysis, Shear Wall, Dynamic Analysis.

ÖZ

DONATILI GAZBETON PANELLER İLE YAPILMIŞ YAPILARIN SİSMİK DAVRANIŞI

Gökmen, Furkan

Yüksek Lisans, İnşaat Mühendisliği Bölümü

Tez Yöneticisi: Prof. Dr. Barış Binici

Eylül 2017, 76 sayfa

Bu çalışmada, donatılı gazbeton panel duvarların ve binaların sismik davranışı incelenmiştir. Elemanlar çevrimsel yanal yükleme ve eksenel yük altında incelenmiş ve sonuçlar önceki testlerle karşılaştırılmıştır. Bu çalışmanın temel amacı donatılı gazbeton panel duvarların ve binaların doğrusal olmayan analizi için öneriler sunmaktır. Hesaplama modellerini analiz etmek için OpenSees platformu kullanılmıştır. Duvarlar fiber kesitlerle modellenmiş olup bu kesitler gazbeton ve çelik donatılardan oluşmaktadır. Çelik donatılar histeretik malzeme ile modellenmiştir. Bu kesitlerin doğrusal olmayan davranışını incelemek için doğrusal olmayan kuvvet tabanlı kiriş-kolon çubuk elemanları kullanılmıştır. Ardından ODTÜ'de daha önce test edilen panel duvarları, artan itme-çekme deformasyonları altında yer değiştirme kontrollü yöntemle analiz edilmiştir. Eksenel yük oranının modeli etkilediği bulunmuştur. Bu nedenle, duvar eksenel yük taşıma kapasitesinin % 10'undan az ve % 10'undan fazla olan durumlar için iki modelleme parametre seti önerilmiştir. Üç artı bir panel sonuçlarını kullanarak

yapılan analizlerin, dört panelli duvar modellerini başarılı bir şekilde tahmin ettiği bulunmuştur.

Ayrıca, tam ölçekli bina testi maksimum üç panelden oluşan gruplar kullanılarak modellenmiştir. Binanın deney sonuçlarını yakalamak için statik ve dinamik analizler yapılmıştır. Daha sonra, yer hareket ivmesi faktörü ile maksimum ötelenme oranı arasındaki ilişkiyi gözlemlemek için artımsal bir dinamik analiz gerçekleştirilmiştir.

Bu tezin başlıca sonuçları: i) Hafif yapısından dolayı gazbeton binaların, tasarım depremleri etkisinde akma öncesi seviyesinde davranmaları beklenmektedir, ii) Aşırı depremler sırasında, gazbeton binaların göçmeden salınımına yardımcı olabilecek bir miktar deformasyon ve enerji sönümleme kapasitesi mevcut bulunmaktadır. Bu sonuçlara dayanarak, gazbeton binalar, sismik bölgelerdeki alçak katlı yapılar için iyi bir alternatif olmaktadır.

Anahtar Kelimeler: Gaz Beton, AAC, Düşey Donatılı Gazbeton Paneller, Donatılı Panel Binalar, Doğrusal Olmayan Analiz, Perde Duvar, Dinamik Analiz.

To my family for their endless support

ACKNOWLEDGEMENTS

I would like to express my deepest gratitude to my supervisor, Prof. Dr. Barış Binici, whose immense knowledge, understanding, and patience contributed to my development as a graduate student. Without his continuous support, guidance, motivation, and encouragement, this research would not be possible. It was a great honor to work with him.

Besides my supervisor, I would like to thank the committee members, Prof. Dr. Erdem Canbay, Prof. Dr. Murat Altuğ Erberik, Prof. Dr. Kağan Tuncay and Assoc. Prof. Dr. Ramazan Özçelik for their time and contributions on this thesis. Their insightful comments and suggestions, along with hard questions directed me to broaden my perspectives for the research.

I would also like to thank fellow graduate students and friends; Alper Aldemir, Zafer Karakaş, Ali Can Tatar, Yasin Özkılıç, Ozan Uçal, Özgür Paşaoğlu, Volkan Emren, Armin Taghipour, Milad Bybordiani, Orkun Karalı, Ahmet Bahadır Koç, Ömer Işıldak, Harun Başaran, Mustafa Onur Koç, Ayberk Aydın, Koray Eskiduman and Mert Keleş for their support and contribution in this study.

I want to thank METU Orienteering and Navigation Team for their support and encouragement during my graduate education.

Finally, I am deeply grateful to my family, Elmaziye Gökmen, Selahattin Gökmen and Berkan Gökmen for their endless support and motivation throughout my educational life.

TABLE OF CONTENTS

LIST OF TABLES

TABLES

LIST OF FIGURES

FIGURES

LIST OF SYMBOLS AND ABBREVIATIONS

ABBREVIATIONS

AAC	Autoclave Aerated Concrete
ITU	Istanbul Technical University
LEED	Leadership in Energy and Environmental Design
LVDT	Linear Variable Differential Transformer
METU	Middle East Technical University
MSJC	Masonry Standards Joint Committee
OpenSees	Open System for Earthquake Engineering Simulation
PEER	Pacific Earthquake Engineering Research Center
TAACA	Turkish Autoclaved Aerated Concrete Association
UT Austin	University of Texas at Austin

SYMBOLS

A_n	net cross-sectional area of a member
A_{si}	area of vertical reinforcement in reinforced masonry and reinforced panel walls
A_{sw}	area of shear reinforcement
A_v	cross-sectional area of shear reinforcement
d_v	actual depth of a member in direction of shear considered
E_{cm}	mean value of the modulus of elasticity of AAC
E_{AAC}	modulus of elasticity of AAC masonry in compression

f'_{AAC}	specified compressive strength of AAC masonry
f_{rAAC}	modulus of rupture of AAC
f_{ck}	characteristic compressive strength of AAC
f_{ctk}	characteristic value of axial tensile strength of AAC
$f_{\text{ctk;0,05}}$	five percentile of characteristic value of axial tensile strength of AAC
$f_{\text{ctk;0,95}}$	ninety-five percentile of characteristic value of axial tensile strength of AAC
f_{cflk}	characteristic flexural strength of AAC
$f_{\text{cflk;0,05}}$	five percentile of characteristic flexural strength of AAC
$f_{\text{cflk;0,95}}$	ninety-five percentile of characteristic flexural strength of AAC
f_{cm}	concrete compressive strength at 28 days
f_{cu}	concrete crushing strength
f_d	design compressive strength of masonry
f_k	characteristic compressive strength of masonry
f_{vd}	design shear strength of masonry
f_{vko}	characteristic initial shear strength of masonry, under zero compressive stress
f_y	specified yield strength of steel reinforcement
f_{yd}	design strength of reinforcing steel
h	effective height of wall
l_w	length of entire wall or of the segment of wall considered in direction of shear force
M_u	factored moment
N	axial loading

N_0	axial load capacity of a section
N_{Ed}	axial load factored with vertical load and earthquake load coefficients
P_u	factored axial load
S_n	section modulus of the net cross-sectional area of a member
s	spacing of reinforcement
t	nominal thickness of member
V_{cr}	flexural cracking strength
V_{Ed}	design value of shear load
V_n	nominal shear strength
V_{ns}	nominal shear strength provided by shear reinforcement
V_{nAAC}	nominal shear strength provided by AAC masonry
V_{Rd}	design value of shear resistance
V_u	factored shear force
γ_M	partial factor for material property
μ_{AAC}	coefficient of friction of AAC
ε_{c0}	compressive strain at maximum strength
ε_{cm}	maximum usable compressive strain of masonry
ε_{mu}	maximum usable compressive strain of masonry
ε_{sy}	yield strain of steel reinforcement
ε_{su}	maximum usable strain of steel reinforcement
ρ_m	mean dry density

CHAPTER 1

INTRODUCTION

1.1. General

Autoclaved aerated concrete (or Aerated Cellular Concrete or Aircrete) has been used as a construction material since the beginning of the 20th century. AAC was invented after a series of patents. Firstly, Hoffman tested and patented the aeration of concrete with carbon dioxide in 1889, and then Aylsworth and Dyer patented porous cementitious mixture using aluminum and calcium hydroxide in 1914. In 1923, Eriksson developed the modern AAC by autoclaving or pressurized steam curing his aerated mixture of limestone and ground slate. After this breakthrough, the first factory was established in 1929. These researches and developments attracted significant attention hence, more refinements to AAC production was later made for optimization. The first reinforced AAC elements, which were panels and lintels, were invented in 1935 (Boggelen, 2014).

In Turkey, during the 1950s the first AAC products were imported from Germany. After the increasing interest in the use of AAC, first factory with technology transfer from YTONG was established in 1963 in Istanbul. Relevant guidelines to regulate the heat insulation standards for AAC was published in 1970, afterward, Turkish Autoclaved Aerated Concrete Association was formed in 1990.

AAC has many advantages such as being lightweight, easy to transport, good insulation, good fire resistance and durable nature; as a result, it became very popular within a short time in the construction industry. Due to its porous structure, it has low density,

low weight and good insulation properties. Although it is a lightweight material, its mechanical properties may meet the durability standards of lightweight concrete.

Figure 1.1 shows the success of AAC blocks for heat insulation during winter and summer (Ozel, 2011). In the research, mostly used masonry elements were tested for heat insulation in winter and summer. The figure shows that AAC was the most successful material among the tested ones.

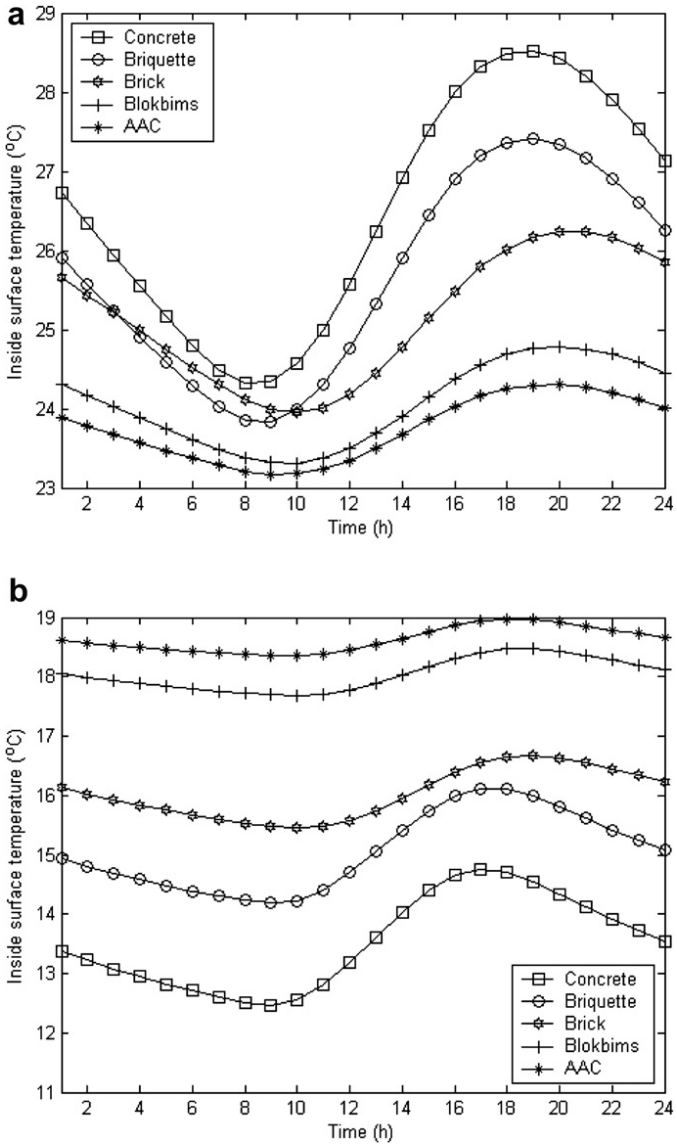

Figure 1.1: Hourly variation of inside surface temperatures of the uninsulated walls: (a) Summer (b) Winter

In addition to its insulation performance, AAC's natural fire resistance property is a good feature for residential and commercial buildings. A wall made from AAC blocks or panels can resist a temperature up to 2000 ^{o}F (1100 ^{o}C) at least for four hours. Percentile change of compressive strength versus increasing temperature is shown in Figure 1.2 (Xella, 2011). At around 800 ^{o}F (427 ^{o}C) temperature, compressive strength becomes maximum and it loses its strength after this point according to the tests done in accordance with ASTM E 119 (ANSI UL 263). As a result of the aforementioned superior properties of AAC, it was started to be used directly for masonry walls and housings. The factory controlled nature of AAC blocks and panels lowers the possibility of construction errors while increasing speed.

The use of AAC is encouraged due to its energy efficient environmentally friendly nature and low cost. Figure 1.3 shows that the consumption of raw materials and energy needed for the production of clay bricks, clay bricks masonry units, calcium silicate masonry units and AAC masonry units (Balkema, 1992). This figure shows that AAC is the most energy efficient construction material among the four masonry units. Therefore, green building certifications like LEED (U.S. Green Building Council) promotes the use of AAC as it is also recyclable.

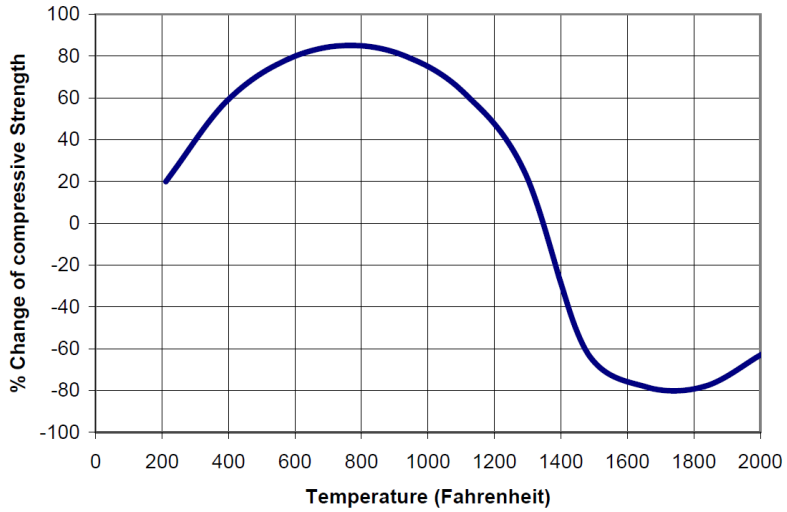

Figure 1.2: Change in Compressive Strength vs. Increased Temperature

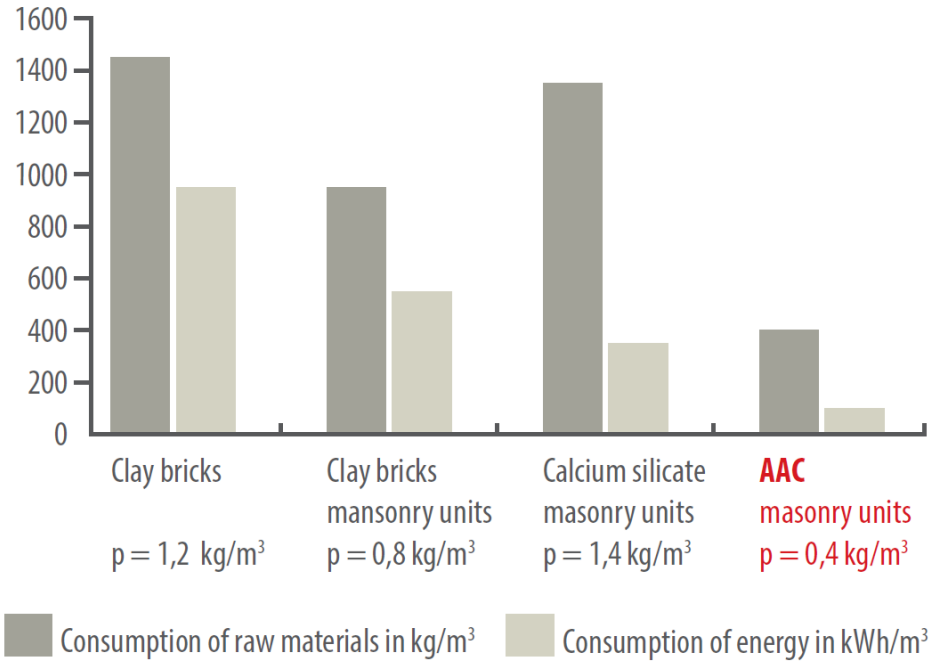

Figure 1.3: Consumption of Raw Materials and Energy Needed for Production

The most important disadvantages of AAC are its water absorption and brittleness. When exposed to water, it directly absorbs water due to its porous form and can experience cracking. Therefore, water coating or plastering should be applied to the surfaces that can be subjected to water or moisture. Due to its brittleness, the producers have developed special coating, mesh reinforcement and plaster agents.

1.2. Production of AAC

Autoclaved Aerated Concrete is a mixture of cement, lime, gypsum, finely grouted sand and aluminum powder as an aerating agent leading to an expansion of the mixture volume up to three times.

Production starts with the grinding of sand and gypsum into powder. This powder is then mixed with water, lime, portland cement and aluminum powder in an automatically weighed mixer. This mixture is then cast into metal molds. The reinforcement mesh with anticorrosive treatment, if there is any, should be placed prior to casting.

Aluminum reacts with the cement slurry to form hydrogen gas, which increases the volume of the mixture and forms the porous structure (Figure 1.4). At the same time, lime and water reaction causes heat resulting in accelerated initial set of cement in about four hours. After this pre-curing process, the self-supporting and semi-solid material is cut with steel wires in wet form for the required element sizes (Figure 1.5).

Afterwards, the elements are cured under steam pressure in autoclaves up to 8-12 hours (Figure 1.6). Then, the elements are removed from the autoclaves, packaged and sent to the storage area. A summary of the production process of AAC is presented in Figure 1.7.

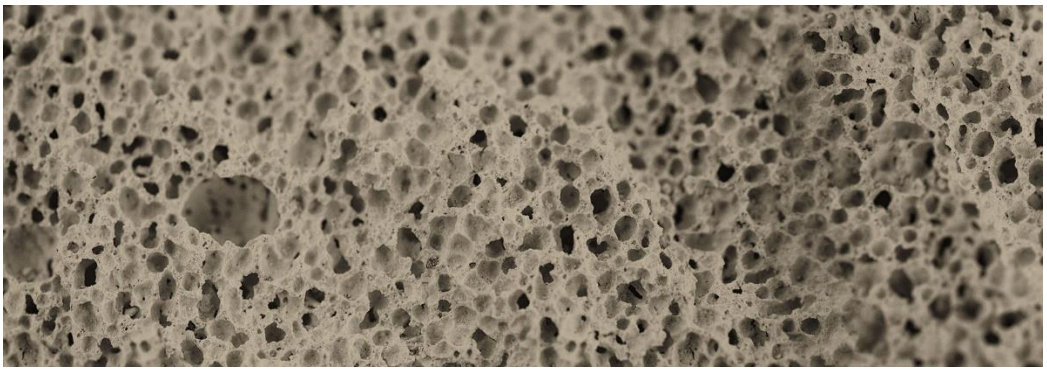

Figure 1.4: Porous Structure of AAC (Imber, n.d.)

Figure 1.5: Cutting Machine with Steel Wires (Xella, 2010)

Figure 1.6: Exterior and Interior Views of Autoclaves (Xella, 2010)

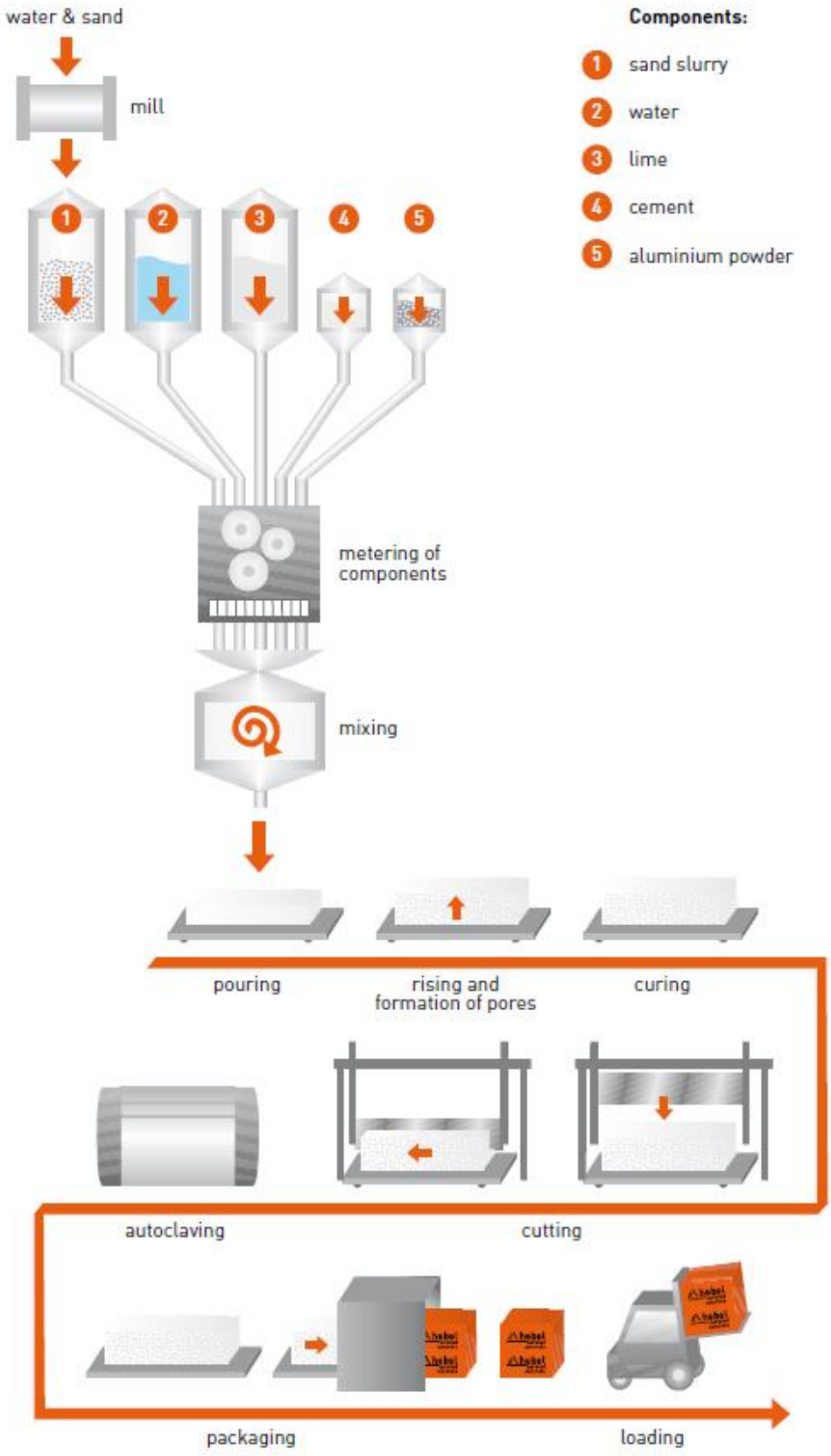

Figure 1.7: Summary of Production Process of AAC (Xella, 2010)

1.3. AAC Elements

Using the processes explained in the previous part, the elements in required forms like blocks (normal, U, round), panels (cladding, partition, load carrying, horizontal, roof, floor) and lintels can be prepared for commercial use (Figure 1.8).

The most commonly used AAC products are the blocks and lintels as the filler walls. In Figure 1.9, examples of AAC products are shown. These are mainly wall or floor panels or blocks for the walls. They are commonly used as exterior and interior walls in residential buildings. Some example buildings made from AAC are shown in Figure 1.10. In factories and high-rise buildings, horizontal and vertical panels are preferred due to the higher speed of installation. In addition, recent types of AAC elements such as load-bearing reinforced walls, floor and roof panels have gained increasing popularity. These elements are all reinforced with steel mesh. Establishing design provisions for AAC building made of reinforced panels have attracted the attention of the researchers since the beginning of the 21st century.

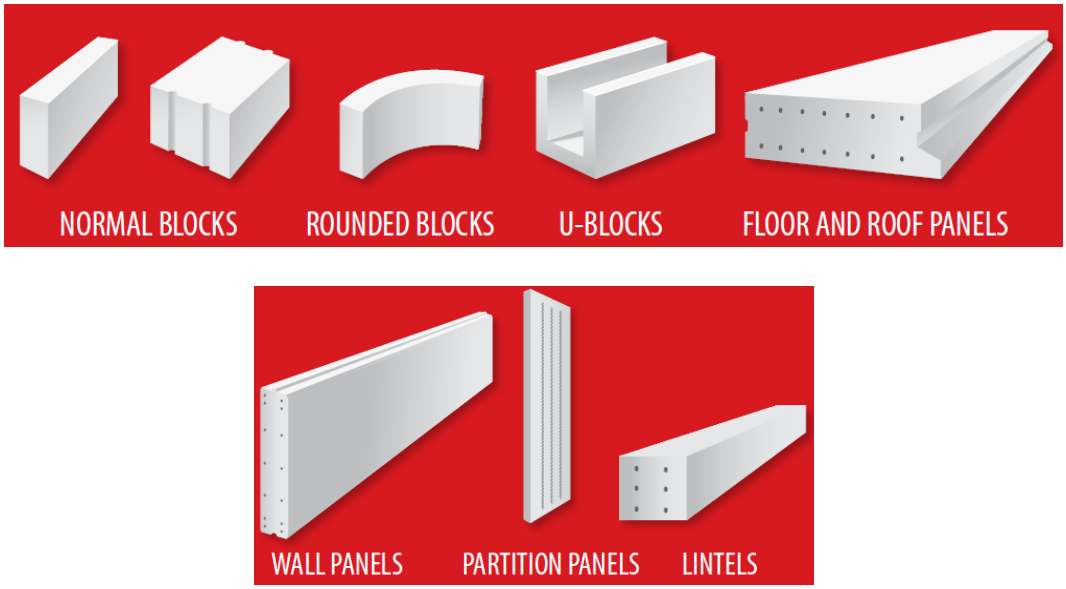

Figure 1.8: Variety of AAC Products (Aircrete Europe, n.d.)

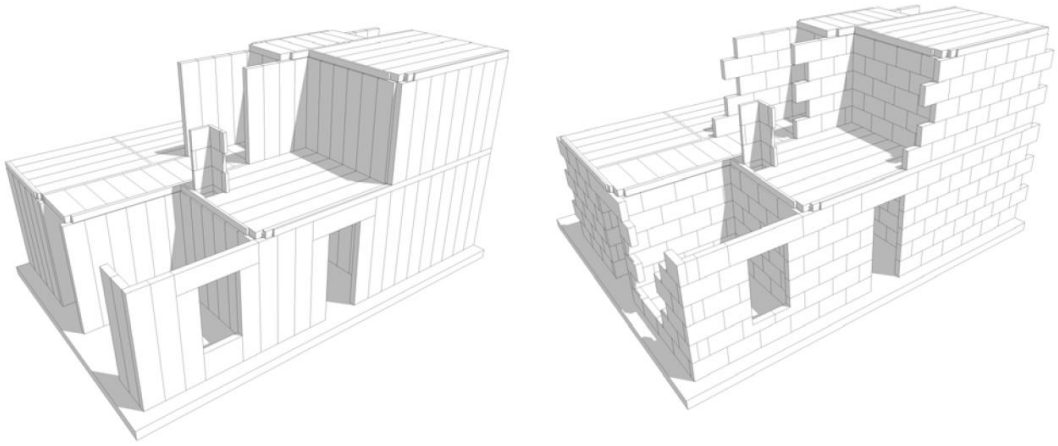

Figure 1.9: Applications of AAC Products (Xella, 2010)

Figure 1.10: Use of AAC blocks and lintels (Myanmar Business, 2017)

1.4. Reinforced AAC Panels

Reinforced AAC panels are generally produced in 6 m length with varying thickness between 100 and 300 mm. The length of the panels can be arranged by saw cutting up to 6 m which is usually dictated by the length of the formwork. Welded wire steel mesh reinforcement is used in reinforced AAC panels with longitudinal bars parallel and transverse to the axis of the panel. Due to the discontinuity of reinforcement in adjacent panels, transverse reinforcement cannot contribute to the shear strength of wall panels, but they are mainly used to provide bond strength.

Panels are placed on a pre-wetted and roughened foundation with leveling bed mortar. The vertical walls transported from the factory are lifted with a special lifting clamp from the short edges as described by the producer (Figure 1.11).

Figure 1.11: Lifting of AAC Panel (Xella, 2010)

The panels are placed on the leveled surfaces and with high precision without any leaning (Figure 1.12). The panels are usually braced with wood or stax sticks. Sufficient setting time is given for the thin bed mortar placed between panel and foundation.

Figure 1.12: Placement of Panel with a Level (Xella, 2010)

If the walls are constructed with vertical reinforcement between each wall, the reinforcement should start from the foundation up to the upper story or they should be lapped with sufficient length. There should be at least a hole diameter of five times the diameter of the vertical reinforcement, which be filled with concrete grout to have sufficient bond transfer between panels and reinforcements to work together. In Figure 1.13, an example of a construction of AAC panel structure is shown. It can be observed that there can be both grouting and thin bed mortar application or one of them according to manufacturer specifications. After the grout application, there is a waiting period for grout curing, after which concrete beams are cast and floor panels are positioned. In Figure 1.14 and 1.15, some example buildings made with reinforced AAC panels are presented.

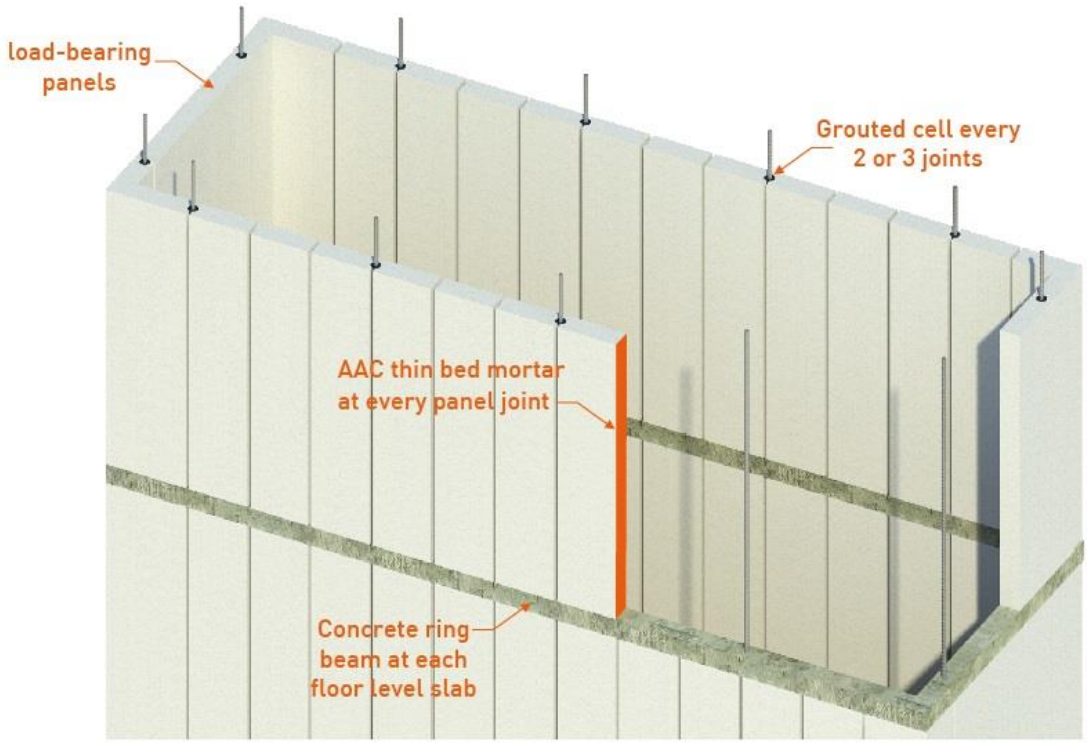

Figure 1.13: AAC Panel Construction Details (Xella, 2010)

Figure 1.14: Example of a Reinforced AAC Panel Building (YTONG, n.d.)

Figure 1.15: Example of a Reinforced AAC Panel Building (YTONG, n.d.)

1.5. Physical and Mechanical Properties of AAC in Reinforced Panels

The AAC properties are defined by the European Standard EN 12602:2015 “Prefabricated Reinforced Components of Autoclaved Aerated Concrete” with the Turkish Translation TSEN 12602. The manufacturers follow this standard for acceptance as a construction material.

1.5.1. Dry Density

In Table 1.1, density classes and mean dry density ranges are presented. The mean value of the results of the six test sets should be within the range of declared density class.

Table 1.1: Density Classes for AAC

Density class	**300**	**350**	**400**	**450**	**500**	**550**	**600**	**650**
Mean dry density ρm	> 250 ≤ 300	> 300 ≤ 350	> 350 ≤ 400	> 400 ≤ 450	> 450 ≤ 500	> 500 ≤ 550	> 550 ≤ 600	> 600 ≤ 650
Density class	**700**	**750**	**800**	**850**	**900**	**950**	**1000**	
Mean dry density ρm	> 650 ≤ 700	> 700 ≤ 750	> 750 ≤ 800	> 800 ≤ 850	> 850 ≤ 900	> 900 ≤ 950	> 950 ≤ 1 000	kg/m^3

1.5.2. Compressive Strength

The compressive strength of AAC is defined by the AAC strength class. Each compressive strength value of the three specimens should give at least 90% of the declared compressive strength. In Table 1.2, strength classes and their compressive strength values are shown.

Table 1.2: Compressive Strength Classes for AAC

Class	**AAC 1.5**	**AAC 2**	**AAC 2.5**	**AAC 3**	**AAC 3.5**	**AAC 4**	**AAC 4.5**
f_{ck} (MPa)	1.5	2.0	2.5	3.0	3.5	4.0	4.5
Class	**AAC 5**	**AAC 6**	**AAC 7**	**AAC 8**	**AAC 9**	**AAC 10**	
f_{ck} (MPa)	5.0	6.0	7.0	8.0	9.0	10.0	

1.5.3. Tensile and Flexural Strength

Tensile and flexural strength should be determined from tests. If the manufacturer does not provide the tests, then the tensile and flexural strength of AAC can be determined according to the following equations:

$$f_{ctk;0,05} = 0{,}10\, f_{ck} \quad (1.1)$$

$$f_{ctk;0,95} = 0{,}24\, f_{ck} \quad (1.2)$$

$$f_{cflk;0,05} = 0{,}18\, f_{ck} \quad (1.3)$$

$$f_{cflk;0,95} = 0{,}96\, f_{ck} \quad (1.4)$$

1.5.4. Other Properties

The strain at design compressive strength is given as 0.002, and the ultimate limit strain is 0.003 according to TS-EN-12602. Modulus of elasticity should be obtained with tests; otherwise, it can be estimated by using Equation 1.5. Poisson's ratio shall be taken as 0.2, and the coefficient of thermal expansion is given as 8E-06 per kelvin.

$$E_{cm} = 5\,(\rho_m - 150) \quad (1.5)$$

1.6. Objectives and Scope

Recently, many different construction techniques and materials are tested and tried in order to obtain energy efficient, fast-constructed and sustainable buildings. A good candidate among them is reinforced AAC panel wall building systems. The New Turkish Earthquake Code (2017) in the process of approval will include guidelines for the construction of AAC buildings in seismic zones. Research on seismic performance of

AAC building is limited as discussed in Chapter 2. Therefore, further research on seismic testing and simulations of AAC structures is needed as they are expected to receive greater attention for low-rise construction in Turkey.

Objectives of this study are:

- To develop computational models to simulate cyclic response of AAC walls
- To calibrate models, simulate the response of tested walls and full-scale building tests
- To critically review of the Turkish Building Earthquake Code by comparing with other design codes, test results and numerical model results.
- To examine the seismic response, deformations and seismic demands of reinforced AAC panel wall building subjected to ground motion.
- To provide recommendations for analysis and seismic vulnerabiltiy of the reinforced AAC panel walls and buildings

1.7. Organization of the Thesis

This thesis is divided into five chapters. In Chapter 2, previous tests conducted on AAC elements structures is presented. Studies of the researchers at University of Texas at Austin and the works at METU on seismic behavior of AAC structures are reviewed in this chapter. Chapter 3 includes seismic design provisions of MSJC (2011) code, Eurocode (2005) and Draft Turkish Earthquake Code (2017). In light of the test results, code provisions are critically reviewed. Chapter 4 describes the numerical modeling strategy for panels and buildings. The computational models are calibrated and building simulation is conducted to observe the seismic response of AAC structures. In chapter 5, conclusions and summary are given. Then, future research recommendations are presented.

CHAPTER 2

AAC PANEL TESTS

In this chapter, previous studies conducted on AAC panels and systems are explained. Firstly, the research project completed at the University of Texas at Austin 15 years ago is presented here. That project covered of testing AAC material, AAC blocks and panels to identify the mechanical properties, testing of AAC walls made with AAC blocks and panels under axial and lateral loads, and the seismic qualification test of a two-story AAC assemblage to understand the seismic behavior of AAC structures to validate design provisions. This was one of the most comprehensive academic studies in the literature on AAC structures in 2003. From that study, only the parts on vertical panel walls are described in the next section due to the relevance of it to this thesis. Secondly, the research project completed in 2016 at Middle East Technical University, Civil Engineering Department, Structural Mechanics Laboratory is reviewed. This project was carried out in order to understand the seismic behavior of AAC structures and to propose guidelines for the Turkish Earthquake Code provisions. Firstly, mechanical properties of AAC material was determined, then reinforced AAC panels were tested under combined axial and reversed cyclic loading. Finally, a full-scale AAC building constructed in the factory of AKG in Kırıkkale and tested under cyclic loads. The results of the project are used herein for the development of the computational model calibration.

2.1. Tests at the University of Texas at Austin (2003)

A comprehensive research program was carried out in order to propose design provisions for MSJC in 2003 at The University of Texas at Austin. Researchers tested firstly

mechanical properties of AAC used for load bearing walls. The reinforced wall specimens were composed of AAC blocks, reinforced panels laid either horizontally or vertically. The shear walls were classified into two groups of failure modes namely shear-dominated and flexure-dominated. This classification was determined by the aspect ratio of walls. Also, a two-story AAC assemblage was tested under lateral loads as a proof test.

The study at UT Austin included the testing of a total of 14 shear wall specimen and a two-story building assemblage. Tests with Specimens 2, 15a, 15b, 16, which are the relevant tests to this thesis, and the two-story assemblage were constructed with vertical panels. Specimen 2 designed as a shear dominant specimen. Specimen 15a, 15b and 16 were the specimens designed to fail in a flexure mode. Vertical axial load was applied on those walls. In Figure 2.1, test setups for Specimens 2, 15a, 15b and 16 are shown. For specimen 2, there were ten panels used side by side and there was no steel reinforcement between them. Specimen 15a had four panels side by side with two 16 mm steel reinforcements at each side closed with 200 mm AAC blocks. Specimen 15b had the same setup with Specimen 15a, the only difference being the use of u-blocks filled with grout at the sides instead of rectangular blocks. The plan views of Specimens 15a, 15b and 16 are shown in Figure 2.2. Reinforcement of all specimens were similar as can be seen from the figures. The AAC had a compressive strength of 4.5 MPa for Specimen 2, and 7.9 MPa for specimens 15a, 15b and 16. The total axial load acting on Specimen 2 was 693.9 kN. The other specimens were under the influence of 111.2 kN of axial load. In Figure 2.3 to 2.5, test results of the AAC panel wall specimens are presented.

The damage observed in Specimen 2 shows that most of the cracks were vertical and flexural cracks (Figure 2.3). The load-deflection response of Specimen 2 is presented in Figure 2.3. It can be observed that the specimen behaved in a ductile manner with a displacement ductility of about 4. During the test, the observed cracks appeared in the following order: Vertical cracks were followed by flexural cracks with simultaneous diagonal cracks and minor spalling. Vertical cracks concentrated around the 3rd and 4th , and the 7th and 8th panels indicating severe separation. The tests with only vertical AAC panels showed that Specimen 2 behaved as a cantilever composed of a series of

panel sets; therefore, the flexural strength of the monolithic wall was not achieved (Figure 2.3.) It should be noted that the shear capacity curves were calculated according to the MSJC (2007) equations which considered web shear cracking and axial load effect. Taking groups of three panels to compute the wall flexural strength was found to give a capacity very close the test capacity. This was the most important conclusion from this test.

The observations for Specimen 15a are summarized in Figure 2.4. Crack formation was due to flexural cracks, flexural-shear cracks and finally vertical cracks. The load-deflection graph of Specimen 16 obtained from the test (Figure 2.5) shows that despite a ductile response, energy dissipation was less than Specimen 2 due to a pinched response. Capacity calculations shown in Figure 2.4 are applicable for both Specimens 15a, 15b and 16. This curve states that taking individual shear capacities of panels and monolithic flexure capacity composed of 4 panels as specimen capacities gave a better approximation for the capacity of flexure dominant walls.

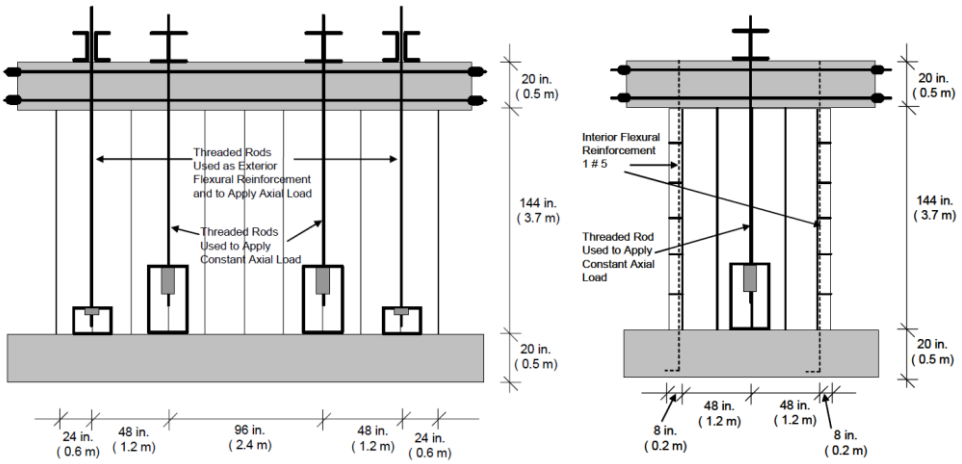

Figure 2.1: Test Setup for Specimen 2 (left); for Specimens 15a, 15b and 16 (right) (Tanner, 2003)

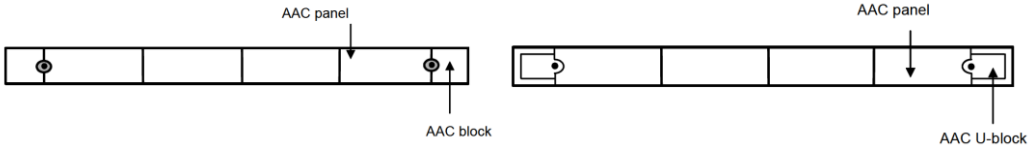

Figure 2.2: Plan View of Shear Wall Specimens 15a, 15b (left) and 16 (right) (Tanner, 2003)

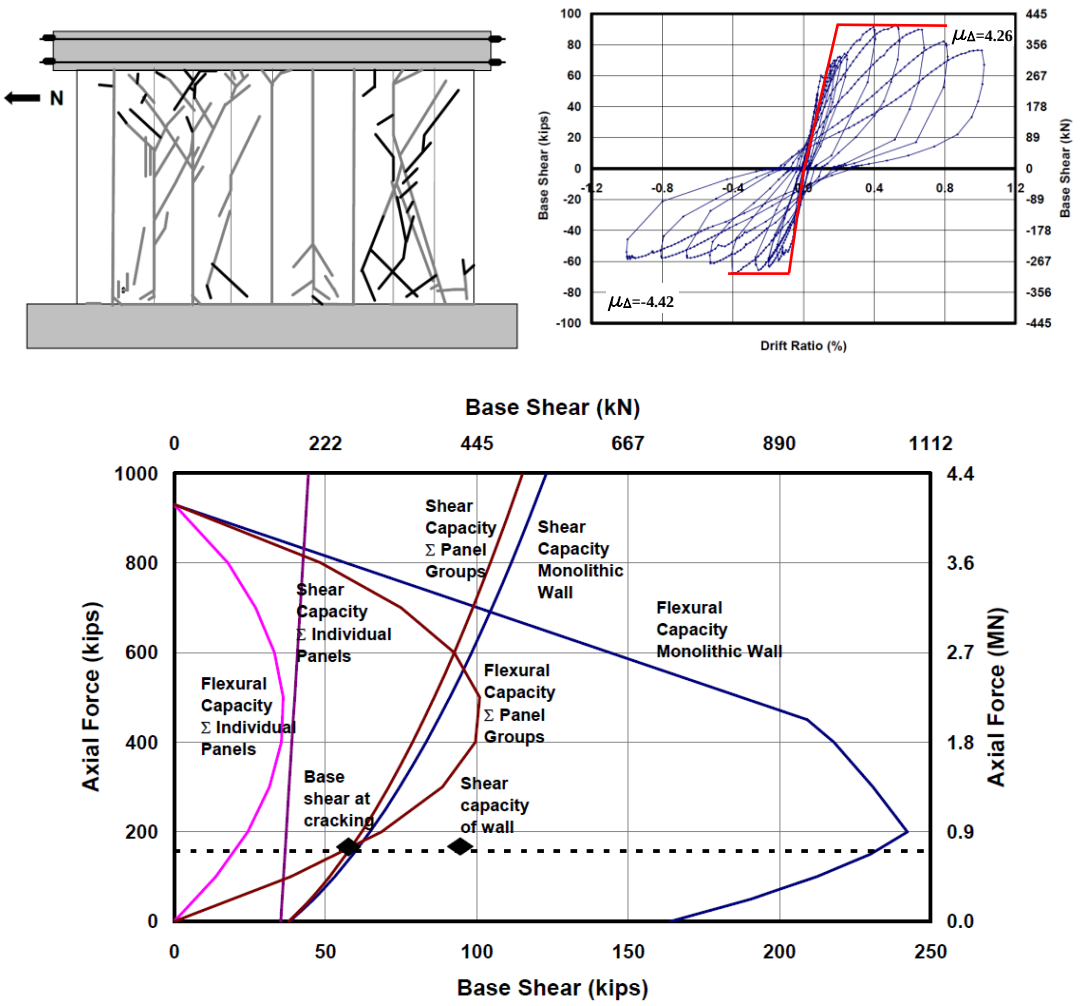

Figure 2.3: Specimen 2 Test Results (top two) & Capacity Curve (bottom) (Tanner,2003)

Figure 2.5 shows the failure mechanism and load deflection response and cracking pattern of Specimen 16. Cracking propagation started with flexural cracks followed by flexure-shear cracks and the crushing of the toe of the wall in both directions. The abrupt loss of stiffness seen in the right figure was caused by the buckling of the reinforcement, leading the crushing of the toes in both directions.

The tests of Specimens 15a, 15b and 16 conducted with four panels and the vertical cracks were observed at the end of the tests. In other words, there was no separation of panels. Therefore, the monolithic response for 4 panels for the flexural strength and

summation of the individual shear strength of panels for wall shear strength observed to be the appropriate way of computing strength. All tests showed that clamping the ends and applying mortar at vertical joints could increase the bond strength of the reinforcement resulting in a better strength than those without clamped ends.

Researchers identified possible failure mechanisms and they related these mechanisms to design equations in order to estimate the load carrying capacities. Observed failure modes were flexural cracking, flexure-shear cracking, web-shear cracking, crushing of the diagonal strut and longitudinal steel yielding. For the specimens constructed from AAC vertical panels, flexural cracking, web-shear cracking, flexural yielding and nominal flexure capacity were the dominant failure modes, for which strength equations were developed.

Contribution of the shear reinforcement was neglected since transverse reinforcement was not continuous. Sliding shear capacity of the wall was affected by the two mechanisms namely, dowel action and friction due to sliding. The proposed equations from the UT study were incorporated in the MSJC code in 2007.

Since the complete research program included different versions of the AAC materials (i.e. panels and blocks) for the construction of the walls, the behavior of reinforced AAC panel walls was not investigated in detail. In other words, more tests with different number of vertical panels and axial loads could provide important information on the seismic response of AAC panels. Although groups of three panels to compute flexure strength was proposed, the number of tests were not sufficient to support this conclusion.

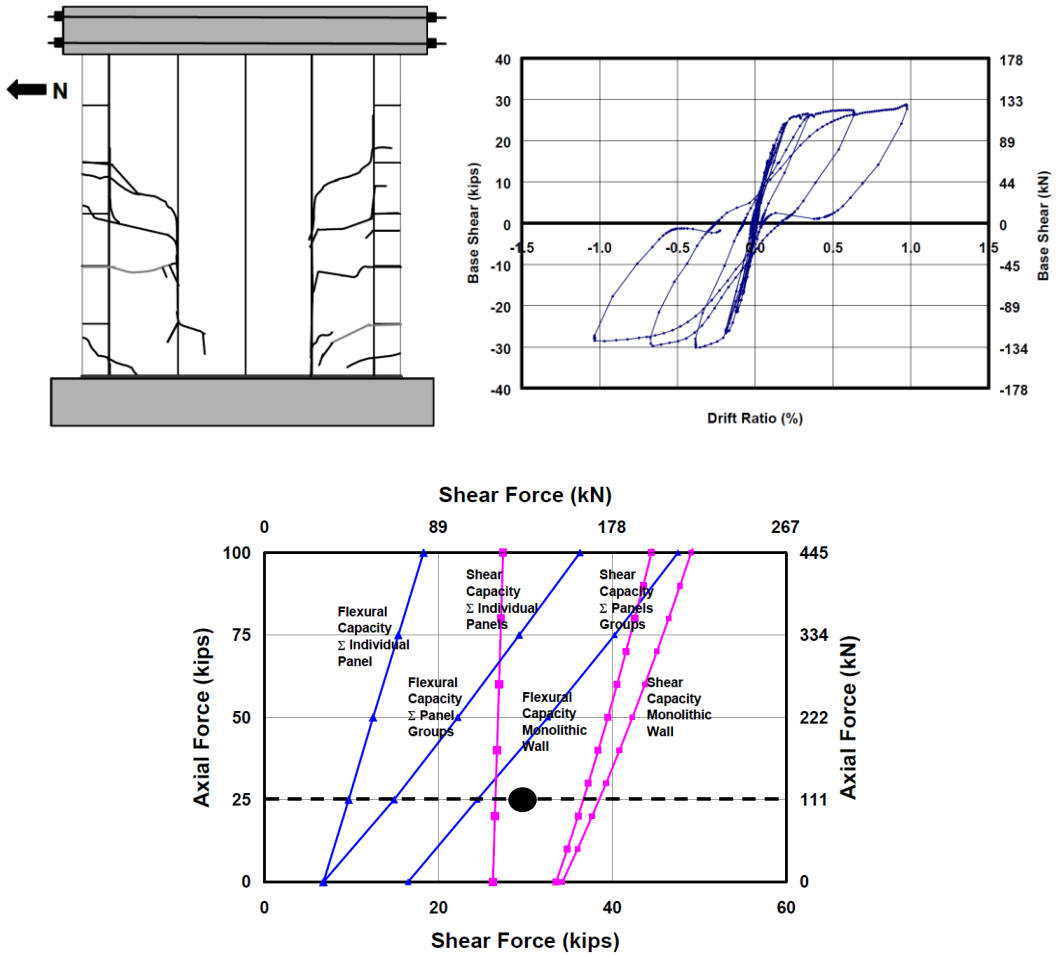

Figure 2.4: Specimen 15 Test Results (top two) & Capacity Curve for specimens 15a, 15b and 16 (bottom) (Tanner, 2003)

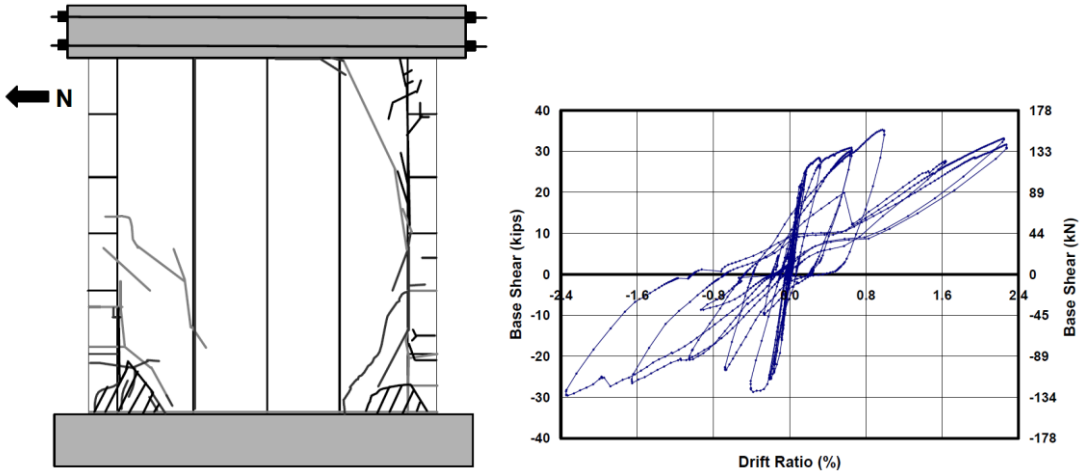

Figure 2.5: Specimen 16 Test Results (Tanner, 2003)

The research program at UT Austin consisted also of a two-story AAC assemblage. The walls were constructed with 10 panels similar to specimen 2 except that there were internal vertical reinforcements at the ends and between the first and second panel on each side. Moreover, there was one panel perpendicular to the north directional walls at the ends. Floor panels were constructed with bond beams on top of the panels. At the first story, floor panels were placed in the east-west direction. At the second story, they were used in the north-south direction. There were longitudinal reinforcements between each floor panel and they are placed inside concrete grouting. In Figure 2.6, three-dimensional view of the assemblage specimen is presented. Load-deflection response of the assemblage is shown in Figure 2.7.

The assemblage was tested under gravity loading of 1330 kN in total and cyclic lateral loading in the north and south directions. The walls showed similar behavior like Specimen 2 and the capacity was close to twice the capacity of Specimen 2 as expected. Displacement ductility was about 4 (averaging two directions). This test showed that buildings with AAC panels could exhibit some ductility. Moreover, the proposed construction method for floors was quite successful. However, the effects of openings in the walls in the loading direction were not investigated and; different combinations of walls, the effects of perpendicular walls and the use of vertical reinforcement between each panel were not investigated.

Within the scope of the UT Research on AAC, Varela (2003) proposed the R and C_d values for the walls and assemblage by using a nonlinear dynamic model. He modeled the walls with a combination of nonlinear shear spring, nonlinear flexural spring and axial spring. He defined the parameters for the springs using the stiffness data of the tested walls. The analysis and test results were compared in Figure 2.8. In these analyses, the capacities were estimated well; however, unloading behavior was realistic after the 0.5 drift ratio. Based on a series of dynamic analysis, Varela derived a procedure to compute R factors. He proposed R factor of 3 for flexure-dominated AAC shear wall structures and 1.5 for shear-dominated AAC shear wall structures; and C_d factor of 3.

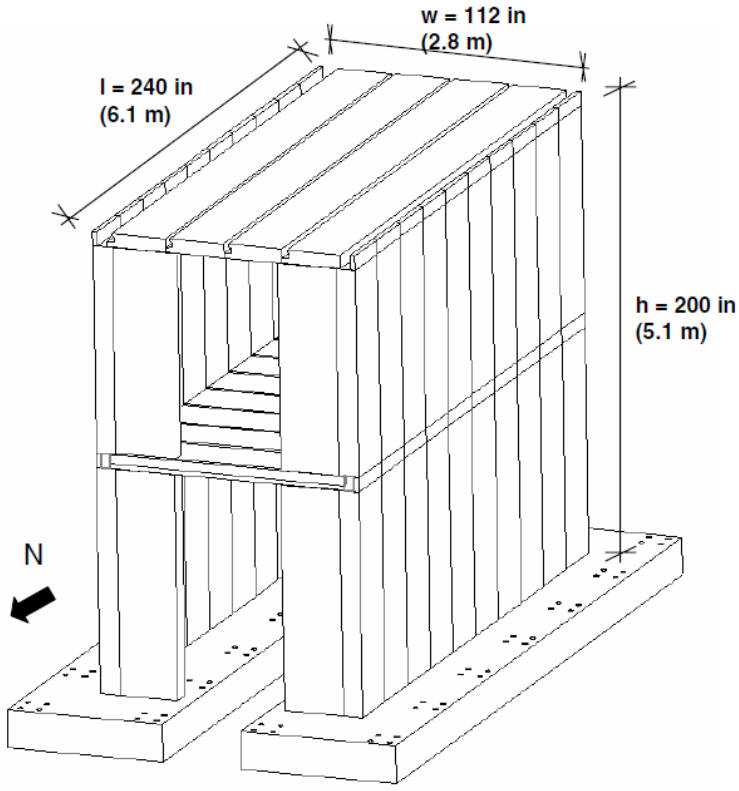

Figure 2.6: 3D view of Two-story Assemblage (Tanner, 2003)

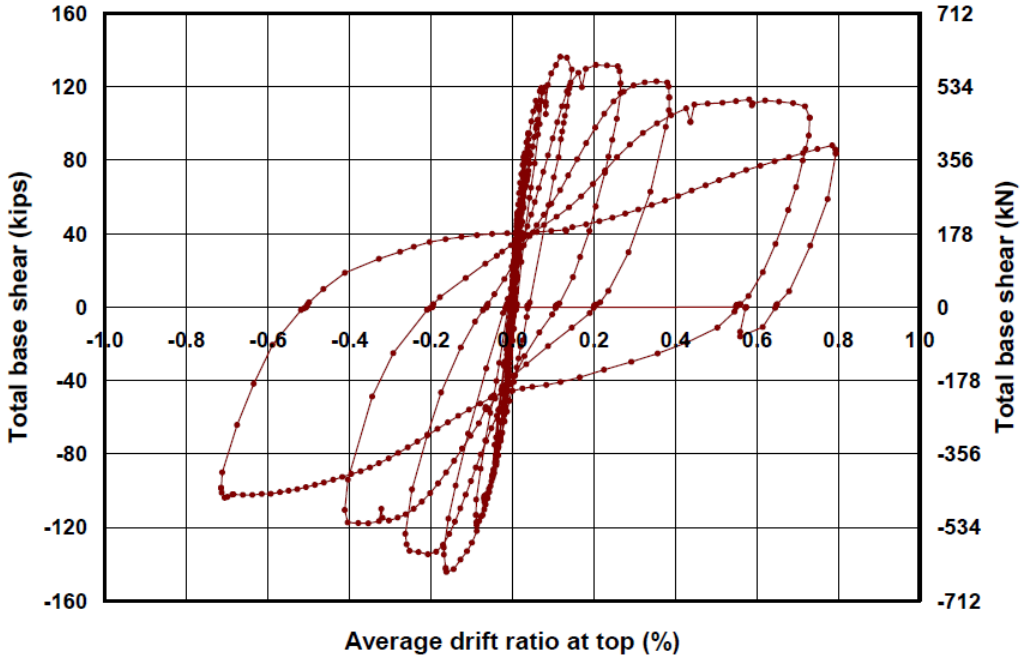

Figure 2.7: Overall hysteretic behavior of Two-story AAC Assemblage Specimen (Tanner, 2003)

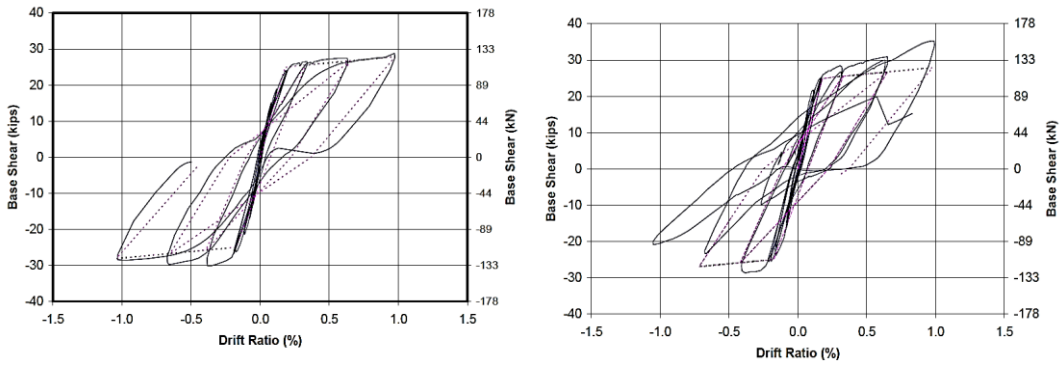

Figure 2.8: Observed vs. Calculated Curves for Specimen 15a (left) and 16 (right) (Varela, 2003)

2.2. METU Studies on the Seismic Behavior of Reinforced AAC Panel Walls (2016, 2017)

Faculty members at Middle East Technical University (METU) and Istanbul Technical University (ITU) initiated a project in 2014 in order to develop seismic design provisions for low-rise buildings built with reinforced AAC vertical panels with the support of Turkish Autoclaved Aerated Concrete Association (TAACA). This project consisted of three parts. In the first part, mechanical properties of AAC was tested at the METU and ITU. AAC block and panel samples were tested under compression, diagonal tension, shear and bending. Moreover, the reinforcement used in panels and at connections were also tested. After these tests, reinforced panel walls and slabs were experimentally studied. The wall specimens were laterally loaded in a cyclic manner to obtain hysteretic behavior, strength and ductility of these elements. Slab wall connections were also tested to examine its seismic safety. Completing the second stage of the project, a full-scale building was constructed with vertical reinforced AAC panels and tested under increasing two way cyclic deformation demands. The building was a full-scale two-story structure and there were reinforced concrete beams between slabs and the panel walls in order to transfer the lateral loads. Displacement controlled loading at story levels was applied to the building at each predefined drift ratios in the positive and negative directions. The applied displacements of each wall group were

recorded by LVDTs pre-installed to the walls. The second and third stages of this project are the main data sources for this thesis.

Taghipour (2016) attempted to investigate the behavior of walls tested within the scope of this project. Within the project, all specimens were made of reinforced AAC vertical panels. In the project, there were six different wall tests. PN1 & PN2 consisted of two panels. PN3 & PN4 had four panels. PN5 was composed of six panels. PN6 was also a six-panel wall with a window opening. The material properties of AAC wall panel elements produced in AAC factory are given in Table 2.1. The reinforcement used between panels had 8 mm diameter with a yield strength of 413 MPa. Each panel had the same dimensions of 600 x 2400 x 200 in mm. PN1, PN3 and PN6 had no additional axial load except the loading beam and self-weight, which was 3.11 kN in total. Loading beam was a 200 x 400 mm reinforced concrete beam. Summary of the dimensions of the specimens is presented in Table 2.2. PN2 and PN4 had axial loads of 120 and 240 kN, respectively. A detailed summary of the applied axial loads on the specimen is given in Table 2.3. The view and details of six specimens are presented in Figure 2.9. Specimens were tested against in a reversed cyclic manner under constant vertical axial load. Base shear versus lateral displacement response of each specimen was measured as presented in Figure 2.10.

The results showed that axial load increased the shear capacity significantly. Also, the base shear capacity did not increase in proportion to the number of panels. The reason was the shear failure domination with decreasing aspect ratio of the specimens. Higher aspect ratio resulted in a flexural failure, lower ones experienced shear failure similar to observed behavior in the tests at the UT Austin. Moreover, openings significantly lowered the capacity and caused the strength degradation due to the complex failure mechanisms.

The observed smallest displacement ductility for specimens (despite flexural failure) values was about 3, which was lower than the seismic response modification factor proposed in the new Turkish Earthquake Code i.e. R=4 for AAC reinforced panel buildings.

Table 2.1: Material properties of AAC wall panels (Taghipouri, 2016)

Type	Dry density (kg/m^3)	f_{AAC} (MPa)	E (MPa)
1	600	4	2250
2	700	4	2750

Table 2.2: Dimensions of the Specimens (Taghipour, 2016)

Specimen	Number of panels	L (mm)	H (mm)	T (mm)	N/N0
PN1	2	1200	2400	200	0
PN2	2	1200	2400	200	0.13
PN3	4	2400	2400	200	0.01
PN4	4	2400	2400	200	0.13
PN5	6	3600	2400	200	0.02
PN6	6	3600	2400	200	0.02

Table 2.3: Applied Axial Loading Details (Taghipour, 2016)

Specimen	Axial Load (kN)	Self-weight & beam (kN)	Total Axial Load (kN)	Axial Stress (MPa)
PN1	0	6.22	6.22	0.02
PN2	120	6.22	126.22	0.52
PN3	0	12.44	12.44	0.02
PN4	240	12.44	252.44	0.52
PN5	0	18.66	18.66	0.02
PN6	0	18.68	18.68	0.02

The final part stage of the project was the full-scale testing of an AAC structure constructed with reinforced AAC panels. In Figure 2.11, the side view of the loading system and test building is presented. The building was loaded in a reversed cyclic manner according to predefined drift ratios (Figure 2.12). Plan views and section views of the test building are shown in Figure 2.13 and Figure 2.14, respectively. There were longitudinal reinforcements between each panel at the walls and floors. There were also

reinforced concrete beams on top of the panels and they were used to connect the floors and panels. There was 4 cm of concrete topping on the floors to simulate in-situ conditions.

The details of the 3D project building (top three figure) and its loading setup (bottom two figure) are shown in Figure 2.15. Top three figures of Figure 2.15 are three-dimensional views of the project building including section views of middle and back walls. At the bottom two figures, test setup is shown. Approximately 70 LVDTs were used to measure the deformations of the structure, and their locations are presented in Figure 2.14. The test was conducted in displacement controlled manner. After reaching each drift ratio value, the test was paused and all the walls were photographed in order to track crack formations and failures at each step. Damage pictures of walls are shown in Figure 2.16.

In Figure 2.17, lateral load versus top displacement curves are presented for the first story, second story and total building. According to the results of the test, at %0.19 drift ratio, maximum lateral load capacity was reached which is 580 kN. It was about 1.6 times the weight of the building. This indicated that the building can resist 1.6g laterally. After reaching the maximum capacity, the capacity decreased by %20 at %0.35 drift ratio resulting in an average ductility of about 3.3. Assuming equal energy principle holds for stiff structures, structural behavior factor can be calculated as 2.35 ($R = \sqrt{2\mu - 1}$).

According to the observations and graphs, deformations were concentrated on the first floor and the deformations were mostly due to flexure with some minor shear cracking. The lateral loading capacity became stable at 310 kN, and deformations increased. The reason for such behavior was that the rigid diaphragm and movement of the elements together with the successful connection system between floor and walls. The building load-deflection response was much more pinched compared to the UT assemblage test. This can be attributed to the presence of realistic openings, floor topping and realistic assemblage as a building.

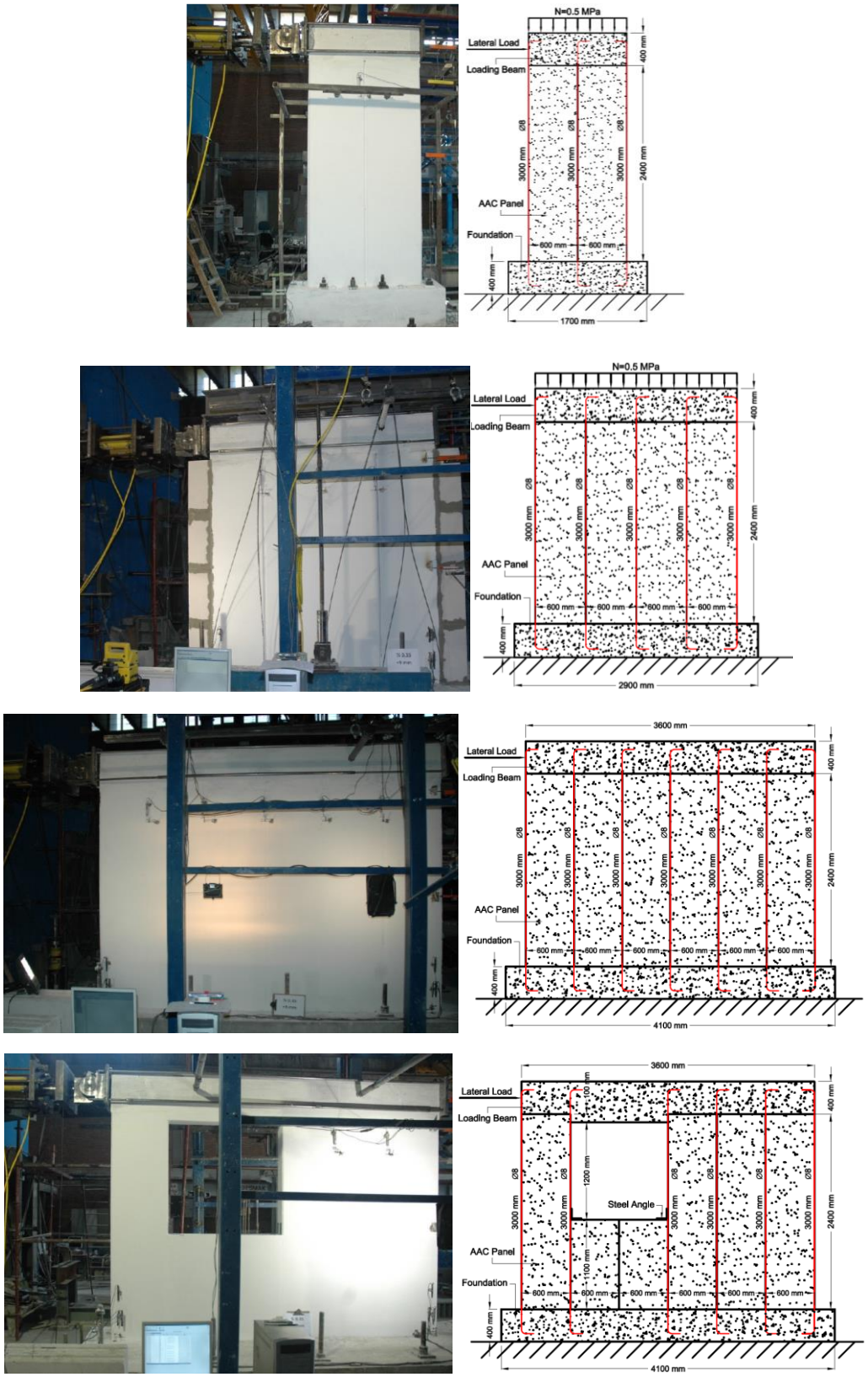

Figure 2.9: Details of the wall specimens (Taghipour, 2016)

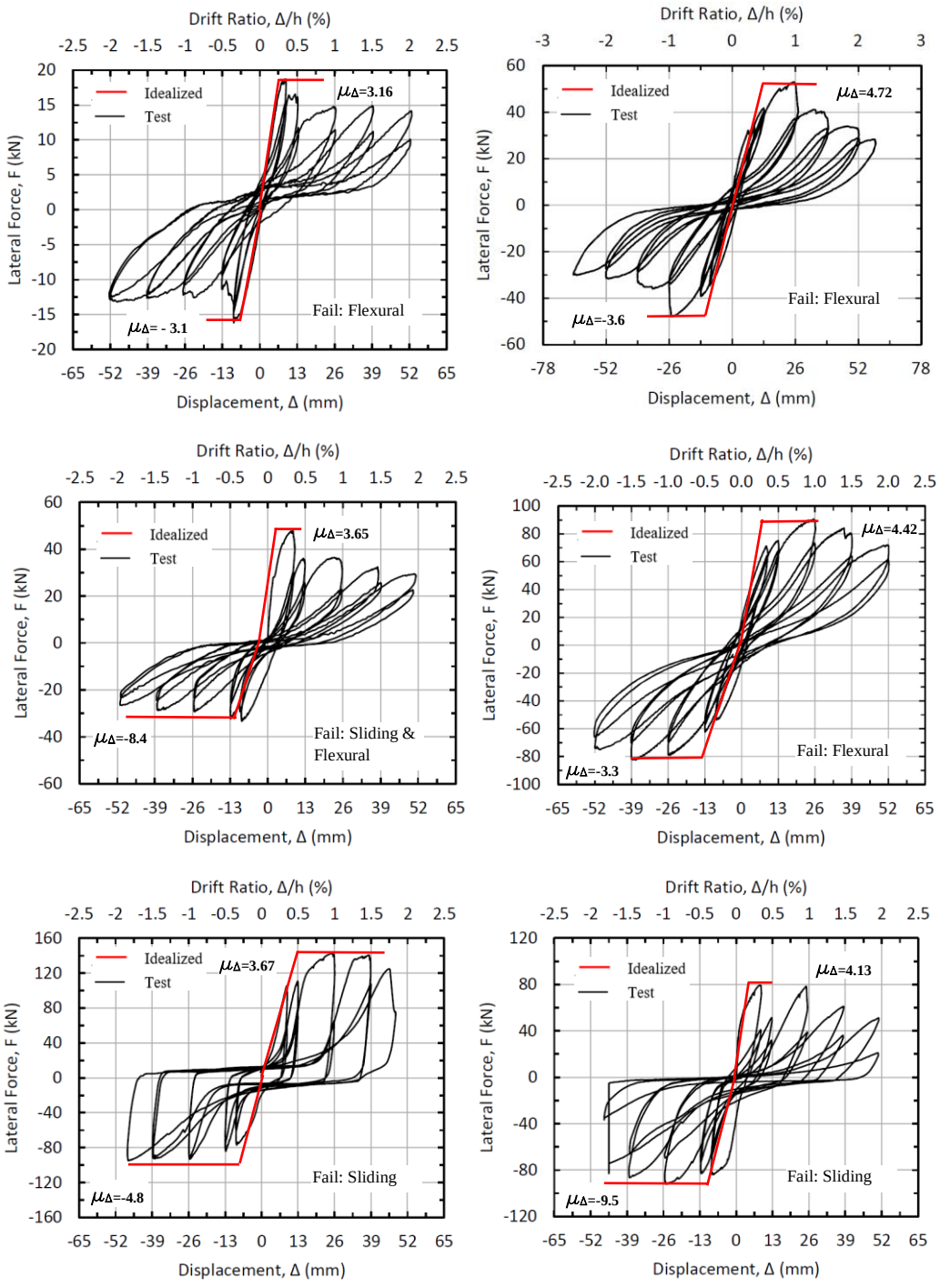

Figure 2.10: Lateral Load vs. Top Displacement Curves for Specimens PN1 to PN6 (left to right and top to bottom) (Taghipour, 2016)

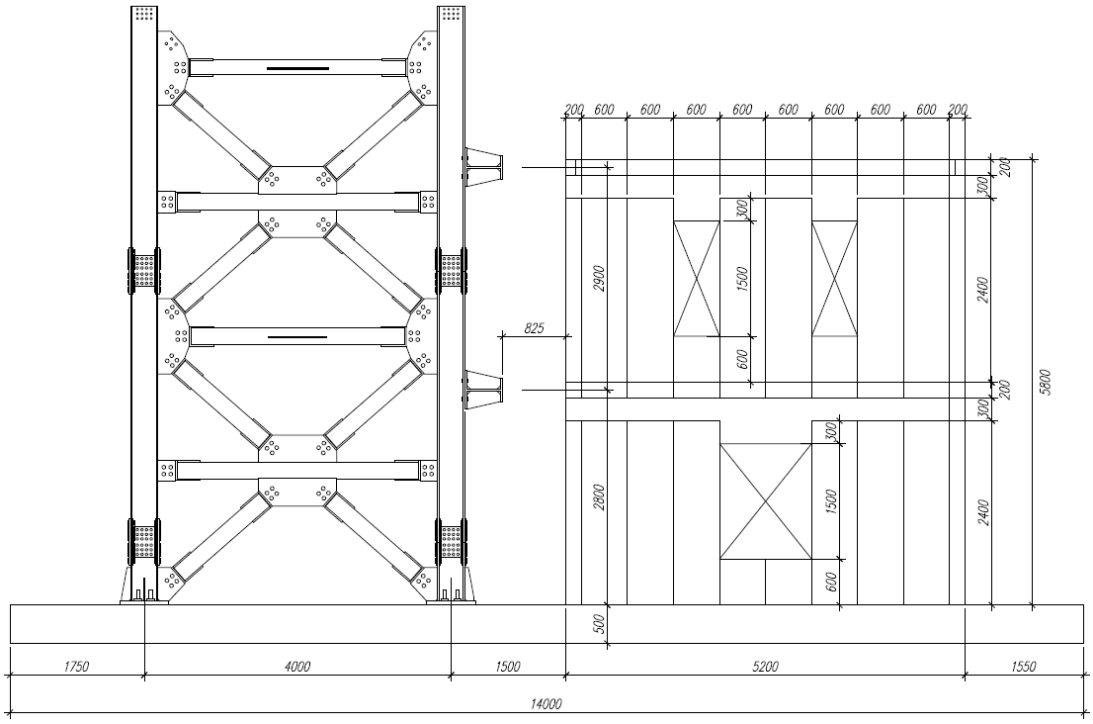

Figure 2.11: Side view of the loading system and the test building

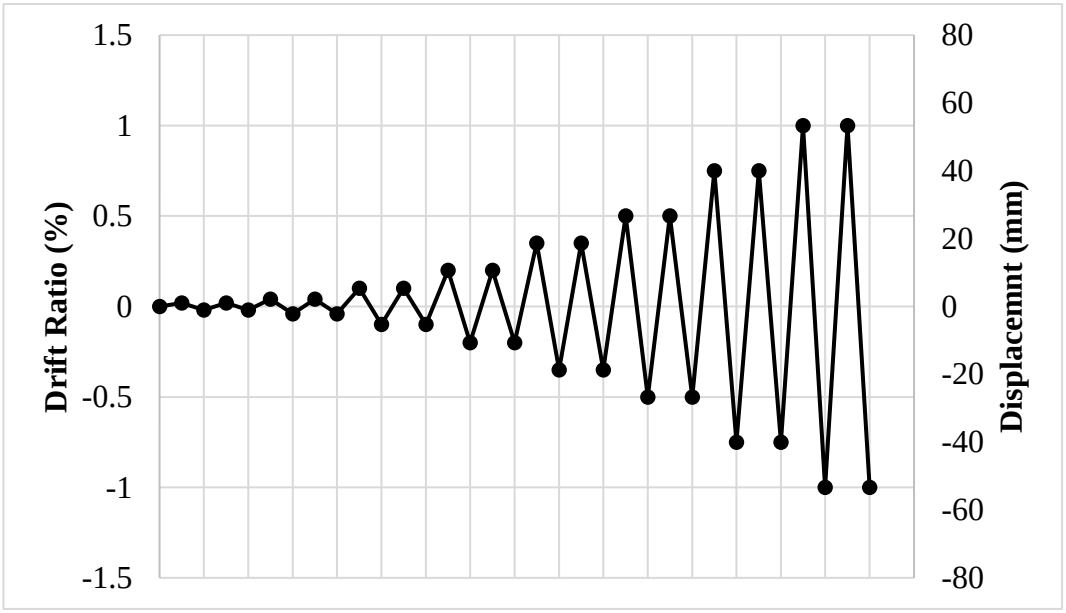

Figure 2.12: Loading History of the Building

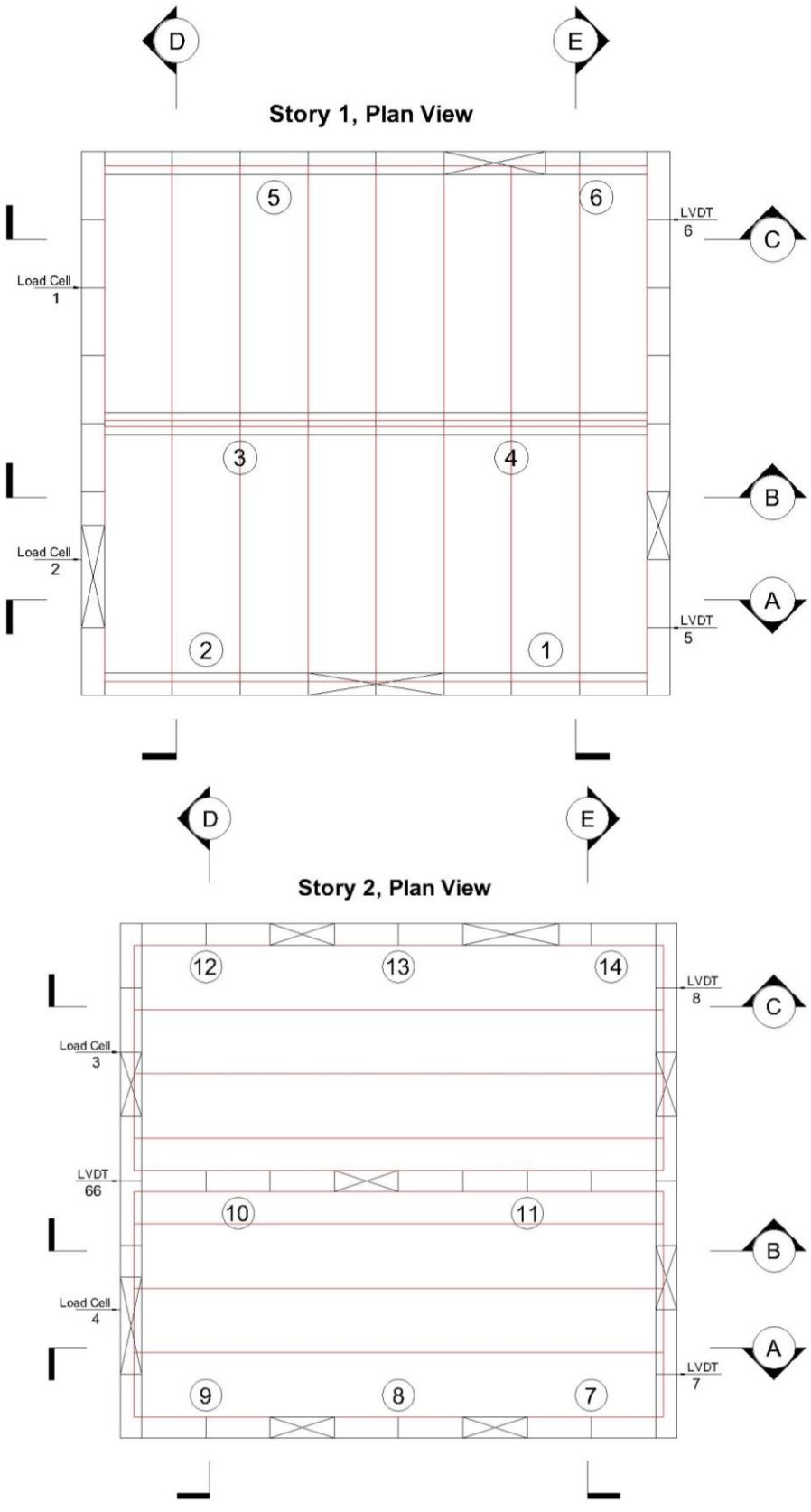

Figure 2.13: Plan Views of the Test Building

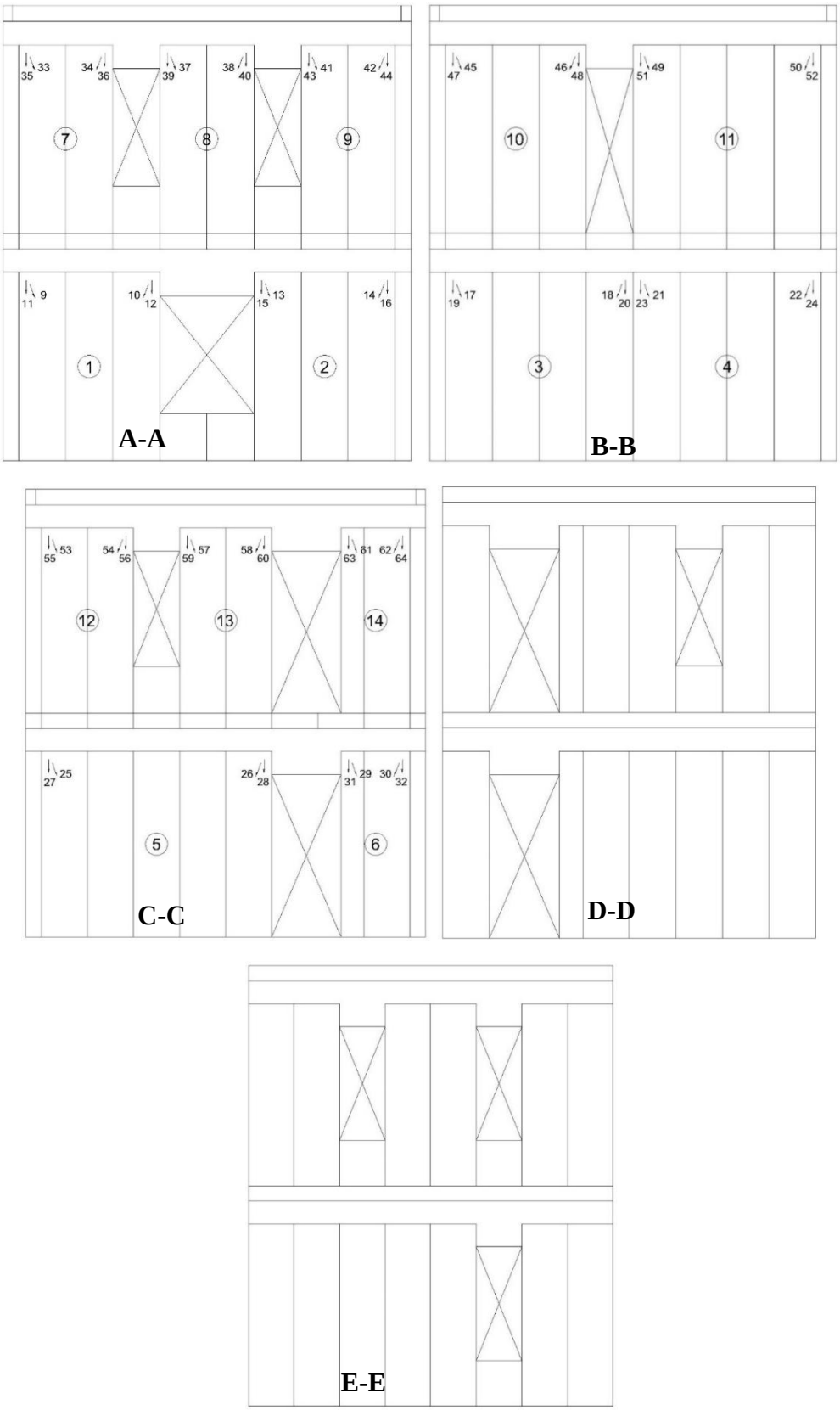

Figure 2.14: Section Views of the Walls & Deformation Measurement Locations

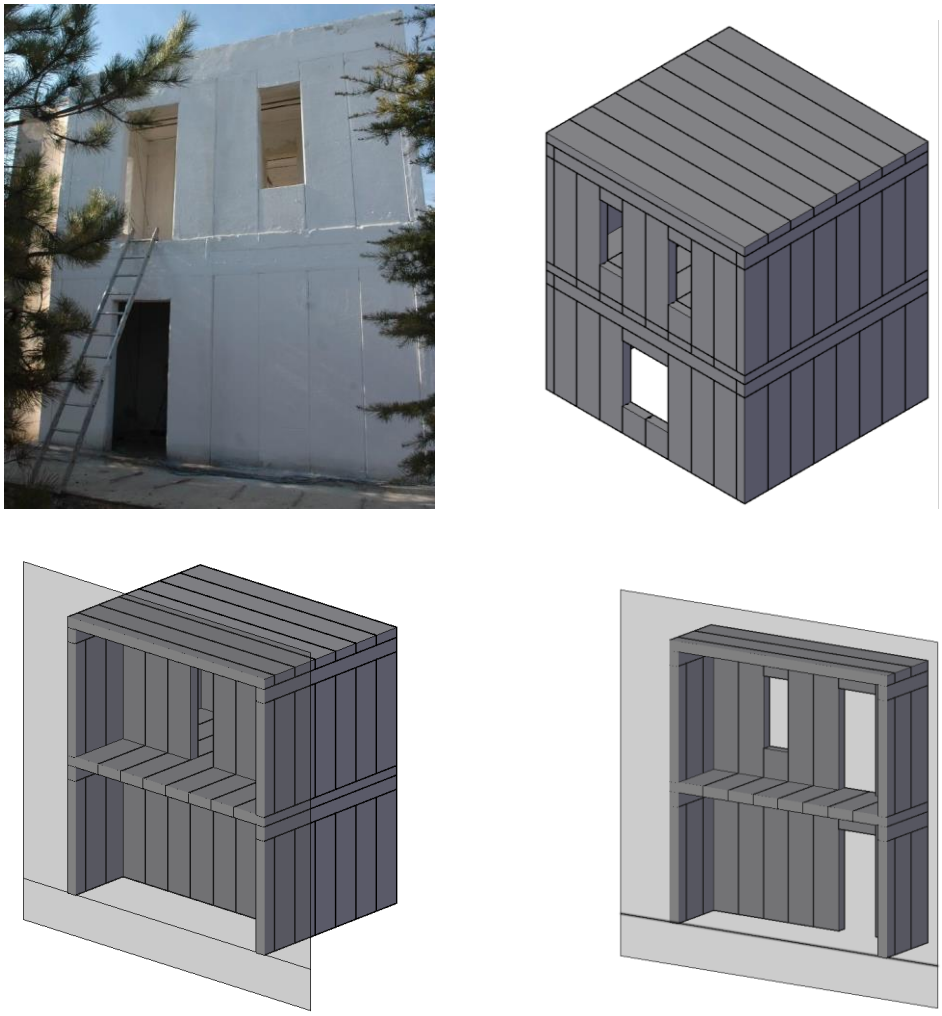

Figure 2.15: Details of Project Building

Figure 2.16: Damage Pictures of Project Building

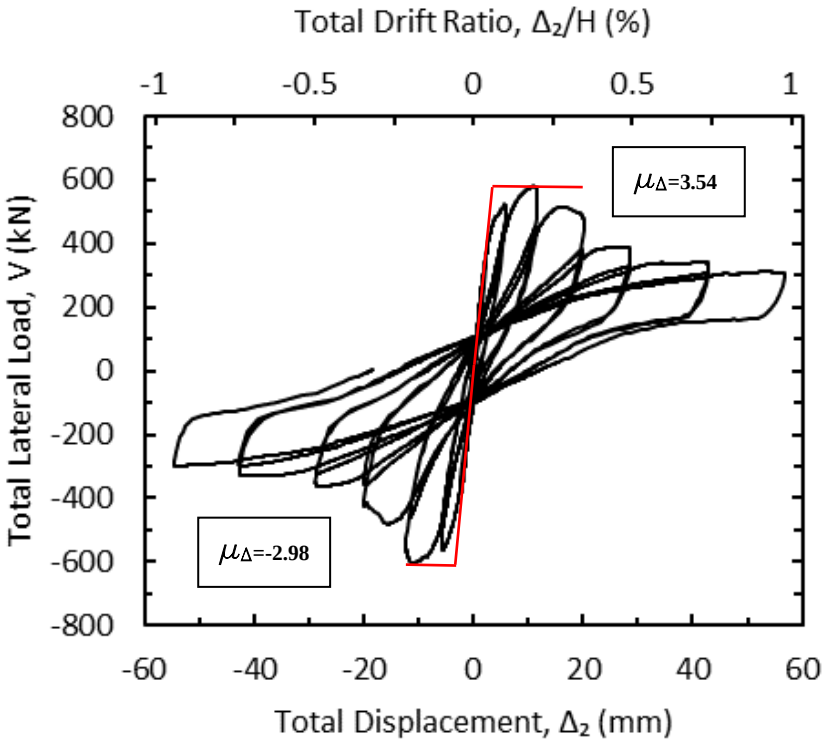

Figure 2.17: Total Lateral Load vs. Tip Displacement and Drift Ratio Curve

The results of the AAC building test provided the following important conclusions:

- The presence of openings results in a pinched response of the building with less energy dissipation.
- The observed ductility was around 3.
- The proposed R factor of 4 in the new TEC (2017) may be on the unsafe side.
- The base shear capacity was about 1.5 times the building weight stating the important advantage of lightweight AAC.

CHAPTER 3

SEISMIC DESIGN PROVISIONS OF BUILDINGS WITH REINFORCED AAC PANELS

In this chapter, three code provisions for the design of reinforced AAC building design guidelines are presented. Firstly, the code requirements offered by MSJC is explained. The provisions for AAC structures mostly developed after the research at UT Austin in 2003. Secondly, the Eurocode design requirements are presented. This code does not have special design equations developed for AAC panels. Thirdly, the new Turkish Earthquake Code is investigated for its design recommendations to build an AAC structure. Finally, in this chapter, the capacity calculations done for shear strength capacity of a shearwall are compared with the capacity results obtained from the tests at UT Austin and METU.

3.1. Building Code Requirements for Masonry Structures by MSJC (2011)

In the United States of America, Masonry Standards Joint Committee (MSJC) published Building Code Requirements and Specification for Masonry Structures to regulate the design of a building with AAC panels. The related chapter of this code is Chapter 8: Strength Design of Autoclaved Aerated Concrete (AAC) Masonry and under this chapter the part 8.3 – Reinforced AAC Masonry. Provisions from MSJC (2011) are presented briefly below.

Modulus of elasticity of AAC masonry is $E_{AAC} = 887.8(f'_{AAC})^{0.6}$. Modulus of rigidity can be taken as 40% of the modulus of elasticity. Modulus of elasticity of grout is 500 times the grout compressive strength. Compressive strength of the AAC masonry,

f'_{AAC}, should be equal or larger than 3.45 MPa, whereas grout must have compressive strength between 13.8 MPa and 34.5 MPa. Masonry splitting tensile strength is taken as 0.2 times the square root of the compressive strength of AAC. Modulus of rupture of AAC is twice the splitting tensile strength. The direct shear strength across of AAC material is 0.15 times the compressive strength and it is taken as 225 kPa between grout and AAC material.

The specified yield strength of reinforcement, f_y, should not exceed 415 MPa and the actual yield strength shall not exceed 1.3 times of f_y. The design assumptions are given in part 8.3.2 of US code for reinforced AAC masonry. The maximum usable strain, ε_{mu}, is assumed as 0.003. 0.85 f'_{AAC} should be assumed uniformly distributed over an equivalent compression stress block bounded by edges of the section and with a line at a distance of a=0.67c from the fiber with maximum strain. The distance c from the fiber of maximum strain to the neutral axis shall be measured perpendicular to the neutral axis. Afterwards, flexural capacity under an axial load is calculated by obtaining c value from equilibrium equations. Groups of up to three panels should be used for obtaining flexural capacities of monolithic walls composed of three and more panels according to suggestions by Tanner (2003) whereas the code does not explicitly state such a requirement.

Nominal shear strength, V_n, is computed with the following:

$$V_n = V_{nAAC} + V_{ns} \tag{3.1}$$

Where V_n should not exceed the following three equations:

$$V_n = \mu_{AAC} P_u \tag{3.2}$$

$$V_n \leq 0.5 A_n \sqrt{f'_{AAC}} \quad where\ M_u/(V_u d_v) \leq 0.25 \tag{3.3}$$

$$V_n \leq 0.33 A_n \sqrt{f'_{AAC}} \quad where\ M_u/(V_u d_v) \geq 1.00 \tag{3.4}$$

Nominal masonry shear strength, V_{nAAC}, is calculated for the masonry not laid in running bond according to the following equation:

$$V_{nAAC} = 0.075\sqrt{f'_{AAC}}A_n + 0.05P_u \quad (3.5)$$

If it is governed by crushing of diagonal compressive strut, it is calculated with Equation 3.6 for the walls with $M_u/(V_u d_v) < 1.5$.

$$V_{nAAC} = 170000 f'_{AAC} t \left[\frac{h(l_w)^2}{h^2 + \left(\frac{3l_w}{4}\right)^2}\right] \quad (3.6)$$

V_{ns}, nominal shear strength provided by shear reinforcement is computed with the following.

$$V_{ns} = 0.5\left(\frac{A_v}{s}\right) f_y d_v \quad (3.7)$$

Flexural cracking strength, V_{cr}, is obtained by using the following equation:

$$V_{cr} = \frac{S_n}{h}\left(f_{rAAC} + \frac{P_u}{A_n}\right) \quad (3.8)$$

3.2. Eurocode 6 & 8 (2005)

Eurocode is accepted and strictly followed by the European Union (EU) countries. Eurocode 6: Design of Masonry Structures (EN 1996) and Eurocode 8: Design of structures for earthquake resistance (EN 1998) have some specifications for the design of reinforced masonry buildings against earthquake not specifically for AAC panels. In part 6.7.2 of EN 1996, the computation of shear strength of a reinforced masonry wall against in-plane horizontal forces is stated. When the effect of any shear reinforcement is ignored, design shear strength is computed by:

$$V_{Ed} \leq V_{Rd1} \tag{3.9}$$

$$V_{Rd1} = f_{vd} t l \tag{3.10}$$

where,

$$f_{vd} = \frac{f_k}{\gamma_M} = \frac{f_{vko} + 0.4 \frac{P_u}{A_n}}{\gamma_M}$$

The material partial factor, γ_M, is taken as 1.7 for AAC according to the table in part 2.4 of EN 1996-1. The characteristic initial shear strength, under zero compressive stress is taken as 0.15 N/mm^2 from table 3.4 in the code. When the contribution of horizontal shear reinforcement is considered, the value is

$$V_{Ed} \leq V_{Rd1} + V_{Rd2} \tag{3.11}$$

$$V_{Rd2} = 0.9 A_{sw} f_{yd} \tag{3.12}$$

For the shear reinforcement contribution is taken into account, it should be

$$\frac{V_{Rd1} + V_{Rd2}}{tl} \leq 2.0\ N/mm^2 \tag{3.13}$$

The maximum usable strain for AAC masonry group is 0.0035. f_d should be assumed uniformly distributed over an equivalent compression stress block bounded by edges of the section and with a line at a distance of 0.85 times x from the fiber with maximum strain. The distance "x" from the fiber of maximum strain to the neutral axis shall be measured perpendicular to the neutral axis. Afterwards, flexural capacity under an axial load is calculated by obtaining x value from equilibrium equations. As it is stated in part 6.6.2. (6) of EN1996, when the reinforcement in a section is concentrated locally, the reinforced section length should be treated with no more than 3 times the thickness of masonry. In other words, for the flexural capacity calculation, only a single panel consisting reinforcement is considered. Then, the summation of individual panel capacities gives the flexural capacity of the wall. In part 9.5 of EN 1998, there

exist recommended geometric requirements for load bearing walls made with reinforced masonry in Table 9.2. It is stated that as the maximum value for the ratio of effective height to the thickness of the wall, $(h_{ef}/t_{ef})_{max}$, is 15; and minimum thickness is 240 mm. Horizontal reinforcement vertical spacings should not exceed 600 mm and vertical reinforcement area in the wall should be larger than 0.08% of gross area of horizontal section of the wall.

3.3. Turkish Earthquake Code (2017/Draft)

Chapter 11 of the New TEC (2017) focuses on masonry structures. Sections 11.4 to 11.6 are related to the design of reinforced masonry buildings. Part 11.4.5 has the similar shear strength equations with Eurocode EN 1996 part 6.7.2; for the design of reinforced masonry walls not specifically for reinforced AAC panels. In part 11.4.6, it is stated that the shear strength of reinforced AAC panel should be the smallest of the following equations:

$$V_{Rd} = 0.15(f_d)^{0.5} lt \tag{3.14}$$

$$V_{Rd} = N_{Ed} + 0.5A_{si}f_{yd} \tag{3.15}$$

$$V_{Rd} = 0.2f_d lt \tag{3.16}$$

where,

$$f_d = \frac{f_k}{\gamma_M}$$

The material factor, γ_M, is taken as 1.75 for AAC according to the table in part 11.2.11 of this code. Flexural capacity calculation of the New TEC (2017) is same as the Eurocode 1996. Only difference is their material strength reduction factors. There are also some rules in part 11.2 and 11.5. The reinforcement between two panels should

be S420 class and should have a diameter larger or equal to 12 mm. Grout diameter should be 5 times the reinforcement diameter. The AAC material should be at least class 5 AAC. If any reinforced concrete parts are used in the construction, the concrete class shall not be less than C25. In Table 11.4 puts some requirements very similar to Table 9.2 of EN 1998. However, Turkish code enforces the use of these rules also for the reinforced panels. For the reinforced panel masonry systems, the effective thickness should be minimum 200 mm and ratio of effective height to the effective thickness shall not exceed 15. Ratio of vertical reinforcement to the gross horizontal section of the panel should be at least 0.08%. This is directly adapted from Eurocode EN 1998 part 9.5.4(6). Vertical reinforcements should have a maximum 600 mm horizontal spacing. In figure 11.6 of Turkish Code the rules are summarized. In figure 11.8 of the new TEC (2017), the connection details for AAC panels are provided.

3.4. Review of the Reinforced AAC Panel Test Results with Code Equations

In this part, the design equations explained before are used to estimate the strength of the test specimens. Then, these values are compared with the test capacities. The capacities of walls were computed based on their shear and flexural strength and they are shown in Table 3.1. The smaller of the two capacities were taken as the capacity according to each code. The mean ratios of estimated to test capacities for each code are also presented in Table 3.2. In Figure 3.1, it can be observed that the best estimation is provided by MSJC whereas TEC (2017) provides the worst estimate. With the decreasing aspect ratio, shear strength capacities of EC6 and TEC increases. In other words, they predicted that flexure failure dominated with decreasing aspect ratio. On the other hand, MSJC states the opposite. According to MSJC, shear failure dominates with decreasing aspect ratio. The research program conducted at the UT at Austin also reported that shear failure was dominant for the walls with lower aspect ratio. As a result, MSJC code predicted the behavior of AAC panel walls correctly. Although EC6 and TEC could not predict the behavior well, they are generally on the safe side with unsatisfactory estimates.

Table 3.1: The Capacity Values of the Codes and Tests (All Units are in kN)

	MSJC		EC6		TEC		Test
	V_{Shear}	$V_{Flexure}$	V_{Shear}	$V_{Flexure}$	V_{Shear}	$V_{Flexure}$	$V_{Capacity}$
PN1	15.05	17.33	39.48	11.08	39.85	11.08	18.70
PN2	27.65	46.69	106.68	26.23	72.00	26.23	53.00
PN3	55.14	40.48	78.97	22.17	48.56	22.17	48.00
PN4	88.99	111.08	213.37	52.45	144.00	52.45	90.90
PN5	82.71	166.67	118.45	33.25	57.26	33.25	142.80
Spe. 15	102.27	120.34	98.40	49.25	223.09	28.98	134.00
Spe. 2	191.01	590.26	334.46	518.72	288.64	517.92	413.00

Table 3.2: Comparison of Code and Test Results

	Ratio		
	MSJC/Test	EC6/Test	TEC/Test
PN1	0.80	0.59	0.59
PN2	0.52	0.49	0.49
PN3	0.84	0.46	0.46
PN4	0.98	0.58	0.58
PN5	0.58	0.23	0.23
Spe. 15	0.76	0.37	0.22
Spe. 2	0.46	0.81	0.70
Mean	**0.71**	**0.51**	**0.47**
St. Dev.	**0.18**	**0.17**	**0.17**

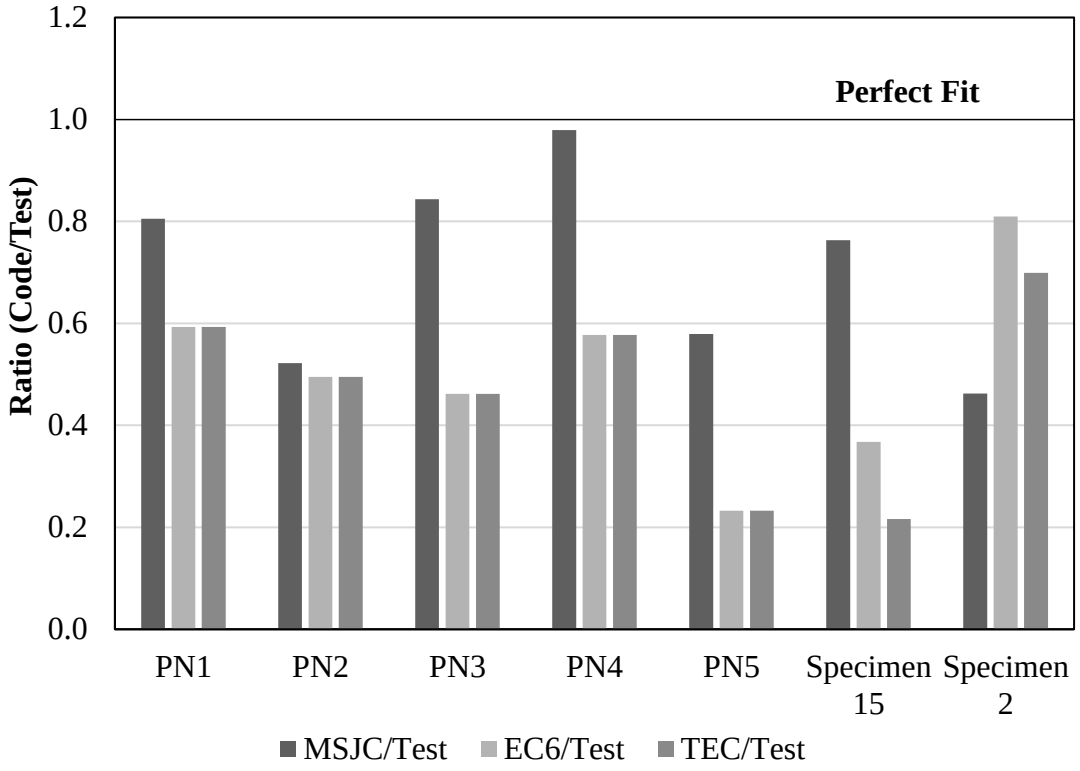

Figure 3.1: Comparison of Code and Test Results

CHAPTER 4

MODELING OF REINFORCED AAC PANELS

Nonlinear modeling of the reinforced AAC panels is essential for the understanding of the seismic performance of AAC buildings. In this work, OpenSees platform is used to analyze the reinforced AAC panels. OpenSees is the short name for Open System for Earthquake Engineering Simulation, and this platform was developed by the Pacific Earthquake Engineering Research Center (PEER) with the support of the National Science Foundation in order to simulate structural and geotechnical systems. To implement material models, solution, data processing and communication procedures, the platform was designed as an object-oriented, modular and extensible work environment. The framework consists of inter-related classes, data structures, models, hierarchical elements, solution algorithms, integrators and solvers. To solve problems with buildings, bridges, soil-structure-foundation interactions and reliability computations, the framework classes are also independent to obtain flexibility in combining modules. OpenSees offers many advantages to researchers to simulate structural and geotechnical systems with realistic nonlinear models by its open-source approach and architecture. Firstly, flexible modeling lets many combinations of element and material formulations with different approximations of kinematics including large displacements and P-D effects. Secondly, to solve stiff nonlinear problems for static and dynamic loadings, there are many alternative solution procedures and algorithms. Moreover, its script language is fully programmable which can be used to define models, solution algorithms and post-process simulation results. Finally, the versatile interface of the framework with networks, databases and storage gives the advantage of high-end computing systems. The structural and geotechnical systems can be analyzed with parallel computing in OpenSees.

4.1.OpenSees Modeling Parameters

To model behavior of the reinforced AAC panels, force-based beam-column elements having section integration points with fiber sections were employed. AAC and steel reinforcement materials were represented with predefined uniaxial materials in Open-Sees library; and, displacement controlled integrator is used for the static cyclic response results of the model to the test results. Afterward, 3D building simulations were performed. Firstly, panels were modeled in two-dimensions with three degrees of freedom per node. Then, selection of the element and material models are explained in detail to show the assumptions of the models and their consequences.

4.1.1. Material

To construct a uniaxial AAC material in compression a non-linear constitutive model and no tensile strength (Concrete01) is used. Typical stress-strain relation is shown in Figure 4.1. For the steel reinforcement representation, a hysteretic model is used. In this way, it was aimed to match pinching of the force and deformation response, damage due to ductility demand and energy, and degraded unloading stiffness based on ductility demand. In Figure 4.2, the employed backbone force-deformation curve is presented. The cyclic response of this model is described later.

4.1.2. Element

Before explaining the details of the beam-column element used for the AAC panels, the section definition should be discussed. In order to model the behavior of AAC panels and the reinforced fiber sections were defined. To decide on the element type representing the section defined above, it is important that tracking the element state at every step of loading and understanding the distributed plasticity and plastic hinge

integration. Therefore, a force-based beam-column element was chosen in order to represent the nonlinearity accurately throughout the analysis.

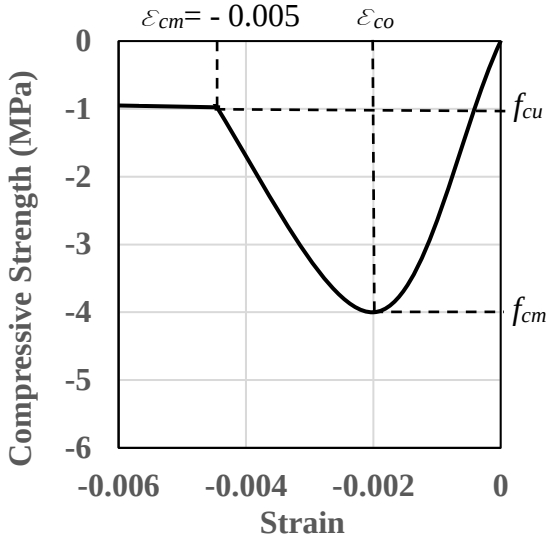

Figure 4.1: Monotonic Stress-Strain curve for AAC material model (METU Test)

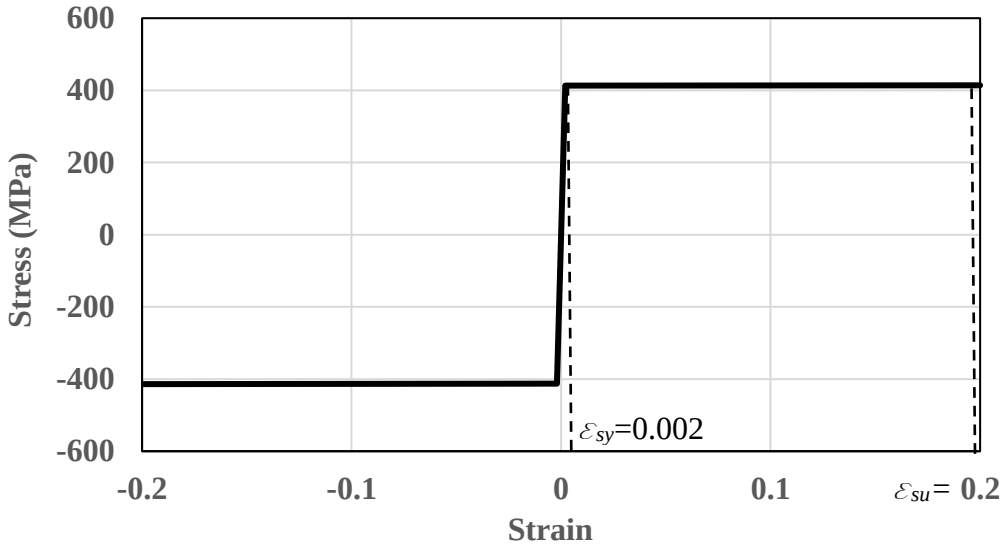

Figure 4.2: Monotonic Stress-strain curve for reinforcement model (METU Test)

4.1.3. Model Parameters

Uniaxial behavior of AAC is presented according to the stress-strain curve shown in Figure 4.1. Ultimate compressive strength and corresponding strain are defined as 4 MPa and 0.002 according to the properties of AAC used in the tests at METU. After ultimate strength, the response is assumed as a nonlinear parabolic curve with a residual strength of 1.0 MPa to overcome convergence problem. Steel reinforcement response is modeled with the stress-strain behavior shown in Figure 4.2. The yield strength of the steel reinforcement used in the tests at METU was 413 MPa with a yield strain of 0.002. In order to simulate the pinched load-deflection curves from panel tests, the steel model was selected as damage hysteretic one. There are four parameters which are *pinchx*, *pinchy*, *damage1* and *damage2*. Pinching parameters, *pinchx* and *pinchy*, are responsible for the pinching of strain and stress during reloading, respectively. They are limited between 0.0 and 1.0 where 1.0 means no pinching. Damage parameters, *damage1* and *damage2*, are responsible for the damage due to ductility and energy, respectively. The damage values are also limited between 0.0 and 1.0 where 0.0 means no damage. Effects of each parameter was investigated. The parameters of the steel model were decided based on load-deflection comparisons with the results of Specimen 2. In Figure 4.3 to 4.7, different combinations of the parameters and their results are shown for the base shear versus top displacement curves. By comparing Figure 4.4 and 4.5, it can be said that *pinchy* value had a significant effect on the behavior of the stress unloading and reloading. By investigating the Figure 4.6 it is obvious that *damage1* parameter is too dominant on the curve and it leads to irregular response hence its effect was ignored by taking it zero. In Figure 4.7, it can be seen that *damage2* parameter affected the reloading part and causes energy dissipation at these steps.

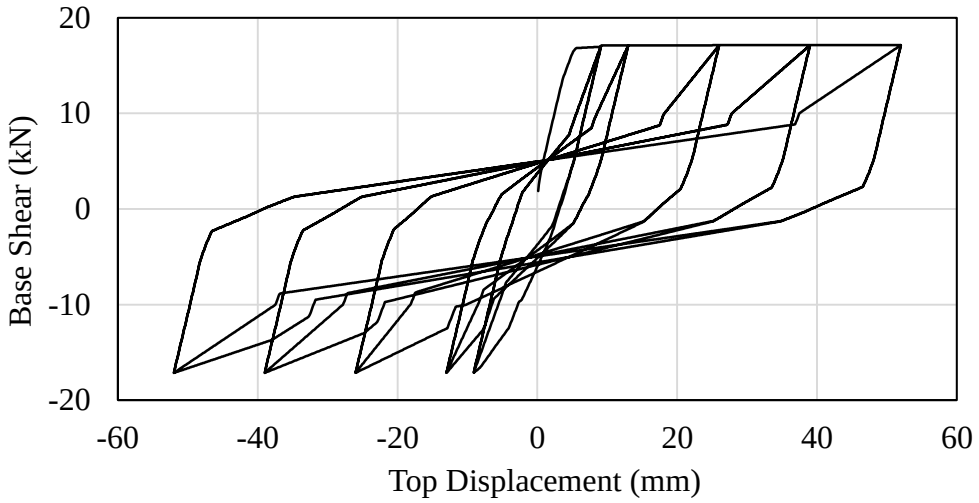

Figure 4.3: pinchx=1 pinchy=1 damage1=0 damage2=0 (default)

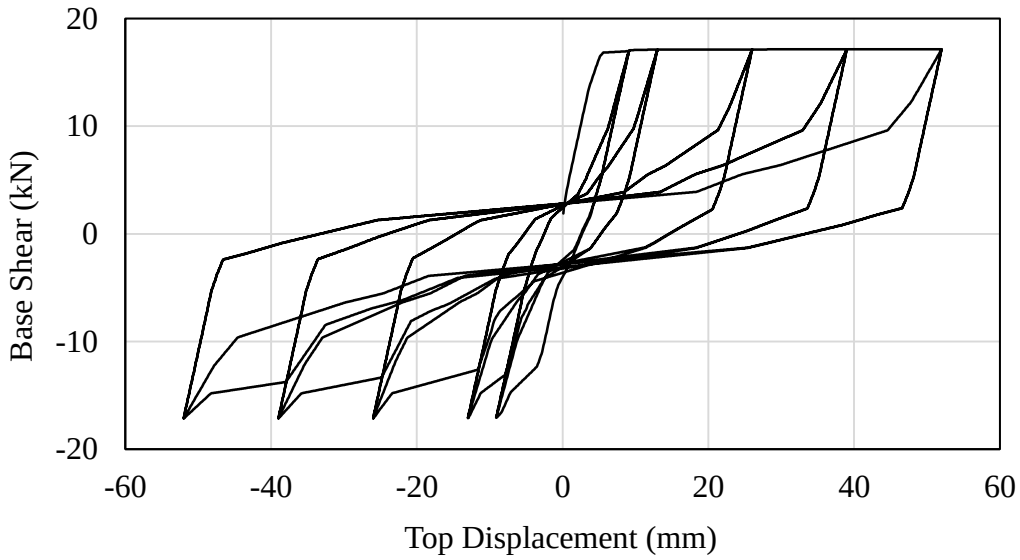

Figure 4.4: pinchx=0.9 pinchy=0.5 damage1=0 damage2=0

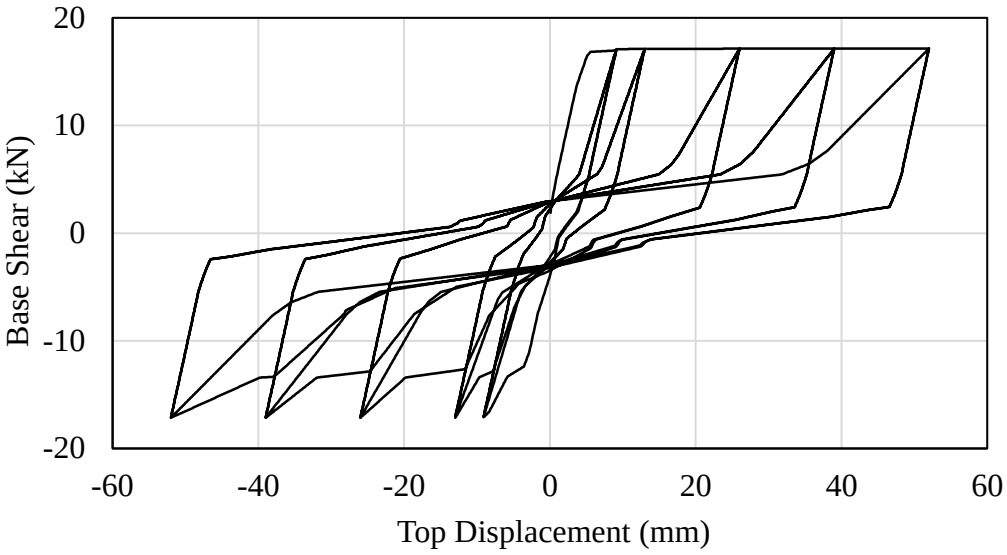

Figure 4.5: pinchx=0.7 pinchy=0.2 damage1=0 damage2=0

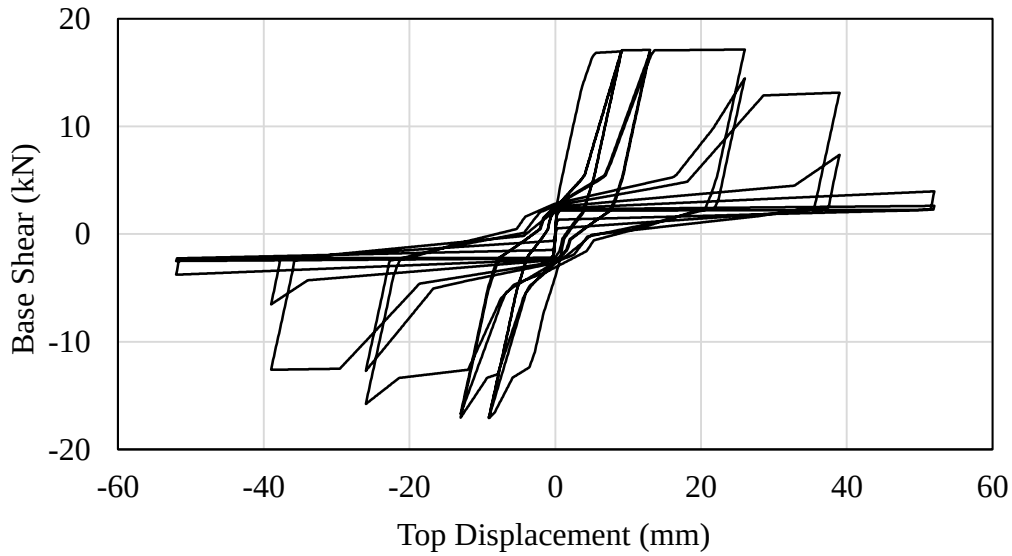

Figure 4.6: pinchx=0.7 pinchy=0.2 damage1=0.02 damage2=0

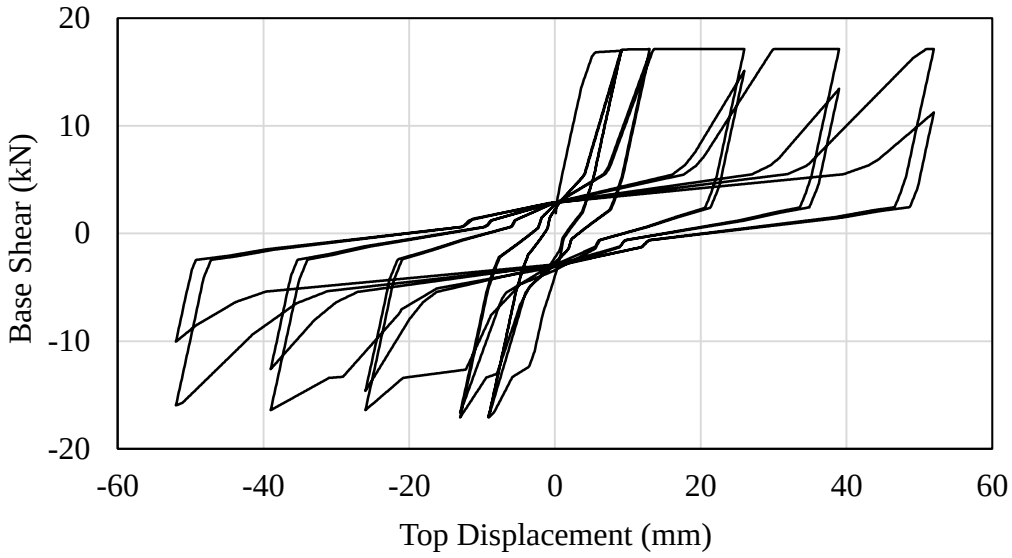

Figure 4.7: pinchx=0.7 pinchy=0.2 damage1=0 damage2=0.2

For the force-based beam columns, five integration points were selected after analyzing two-panel Specimen, PN1, with different number of integration points from 3 to 6 and 50x50mm AAC fibers according to catching the reloading capacity results of test. The integration points analysis results are shown in Figure 4.8. Utilizing five integration points, again PN1 was analyzed with different combinations of fiber sections. The section was 200x1200 mm and the fiber combinations were 2x12, 2x24, 4x48, 8x96, 8x48 and 16x96 accordingly. From these six fiber combinations, 4x48 was selected due to its strength degradation simulation and calculation speed. The fiber section analysis results are shown in Figure 4.9. The integration method was Gauss-Legendre Integration and it places n integration points along the element. The order of accuracy is 2n-1. The location and weight of each integration point are tabulated in *Handbook of Mathematical Functions with Formulas, Graphs, and Mathematical Tables* which was written by Abramowitz and Stegun in 1972.

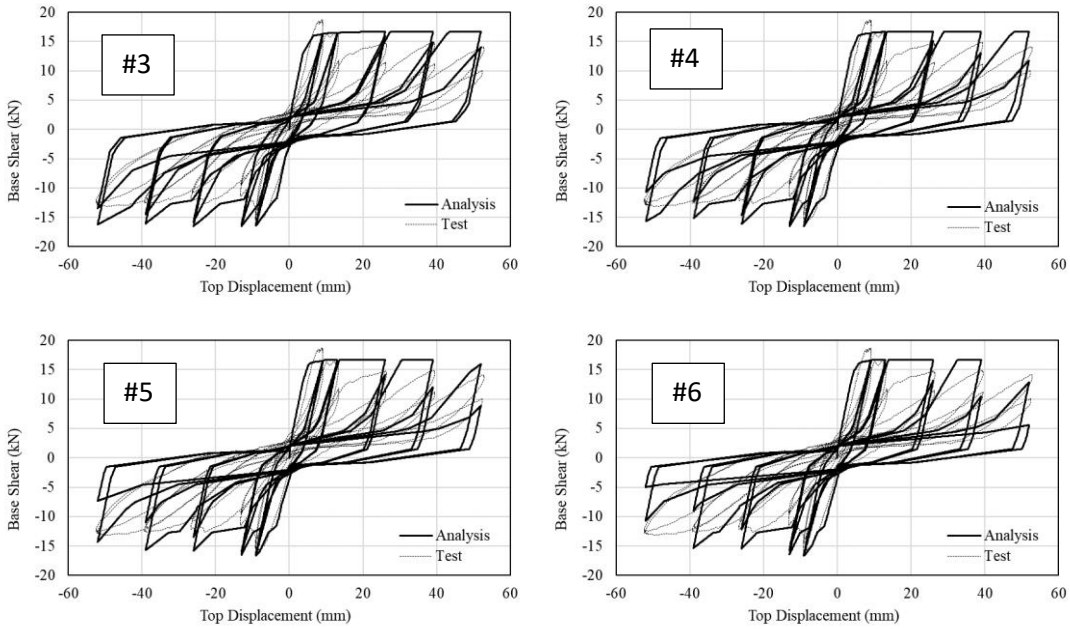

Figure 4.8: Integration Points Analysis Results

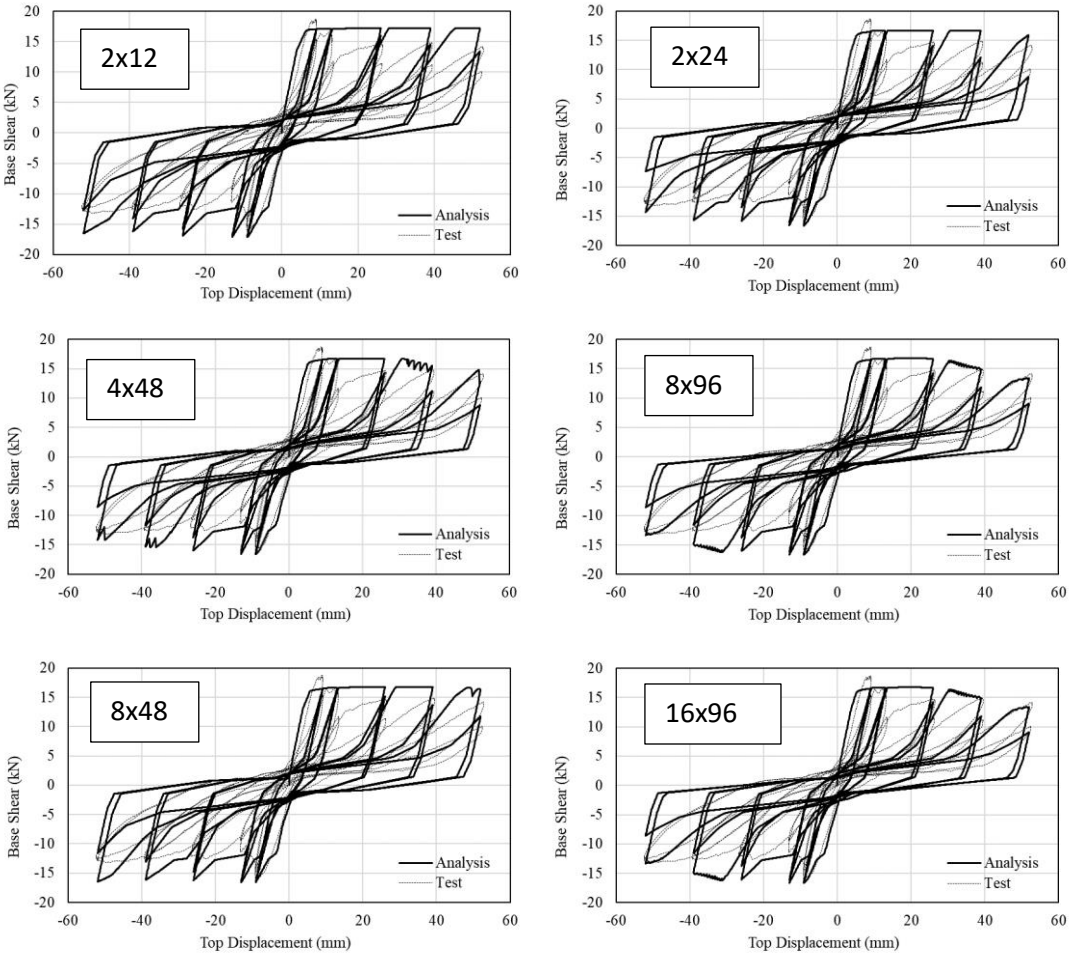

Figure 4.9: Fiber Section Analysis Results

4.2. Comparison of Analysis and Test Results of the METU AAC Panel Walls

In this part, using the selected parameters, the analyses of the test panels were conducted. The base shear versus top displacement curves were taken as the key comparison tool. In Figure 4.10, modeling representation for the two-panel specimen is shown. In this example, firstly fiber representation is decided (bottom right figure) and it is defined as a section of a nonlinear beam-column element (top right figure). In the one portion of fiber representation figure, larger solid circles are the reinforcement locations; smaller circles in the square meshes are the fibers of AAC material. Similar modeling standards was used for all panels and building. Panels are discussed in two parts based on axial forces. For axial load ratios (N/N_0) lower than 10%, response of PN1, PN3 and PN5 were calibrated according to hysteretic parameters of steel reinforcement. For axial load ratio larger than 10% default hysteretic parameters for steel was along with a no-softening curve for the compressive behavior of AAC to avoid convergence problems. PN2 and PN4 were then analyzed.

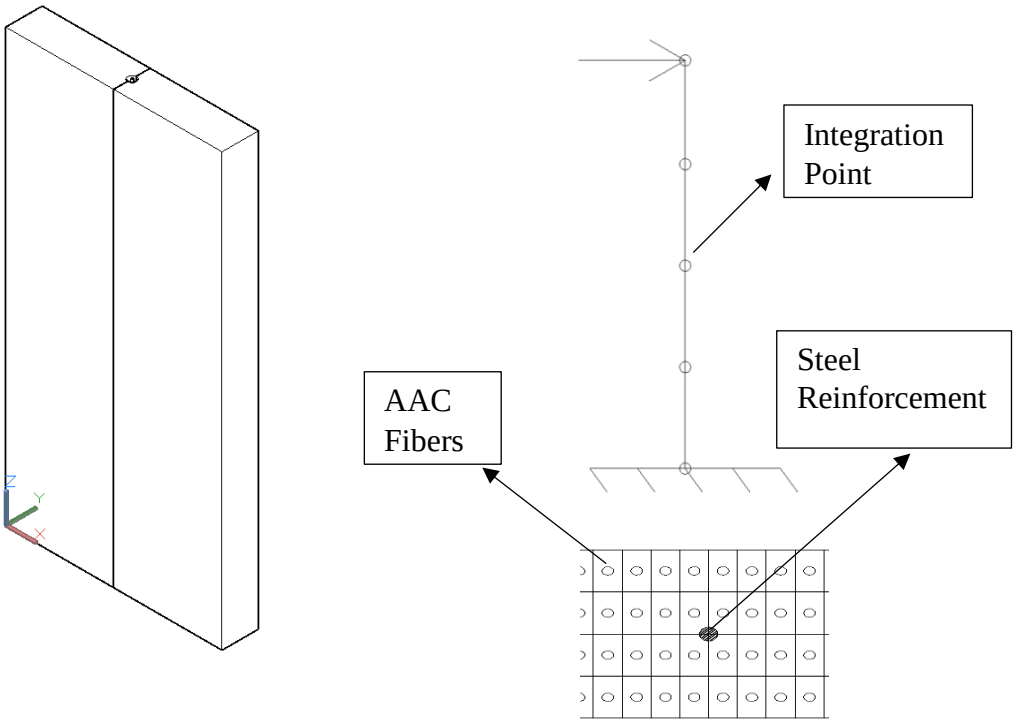

Figure 4.10: Modeling Details of a two-panel wall

4.2.1. Panels with Small Axial Load Ratio { $(N/N_0) < 10\%$ }

4.2.1.1. Specimen PN1

In Figure 4.11, analysis and test results of PN1 specimen, which is a two-panel reinforced AAC wall, are presented together. Ten parametric analyses were conducted to obtain the best match with the test result. The parameters used in each model is shown in Table 4.1. Concrete was modeled with the curve shown in Figure 4.1. Model 1 consisted of default parameters of the hysteretic steel model (Figure 4.11). This model lacked any pinching and it provided an unsatisfactory response. In order to overcome this, *damage2* parameter was selected according to its stiffness degradation effect; and on the curves, *damage2*=0.25 was found to be the optimum match. Furthermore, *pinchy* parameter, when selected as 0.2, estimated the behavior satisfactorily. Next, taking *pinchx* as 0.7 provided better pinching on the curve than the *pinchx* 0.55. Therefore, the best fitting curve parameters were selected as *pinchx*=0.7, *pinchy*=0.2, *damage1*=0 and *damage2*=0.25 according to strength match. The best fitting response model is found as Model 7 in Figure 4.9. The shear capacity obtained from the test was 18.27 kN and analysis shear capacity in Graph 9 is 17.14 kN. An error of 6% for estimating the shear capacity was found.

Table 4.1: Hysteretic Material Parameters for Each Model in Figure 4.11

Model	*pinchx*	*pinchy*	*damage2*
1	1.00	1.00	0.00
2	0.90	0.50	0.00
3	0.70	0.20	0.00
4	0.70	0.20	0.00
5	0.70	0.20	0.20
6	0.70	0.20	0.30
7	0.70	0.20	0.25
8	0.70	0.30	0.25
9	0.55	0.20	0.25
10	0.55	0.30	0.25

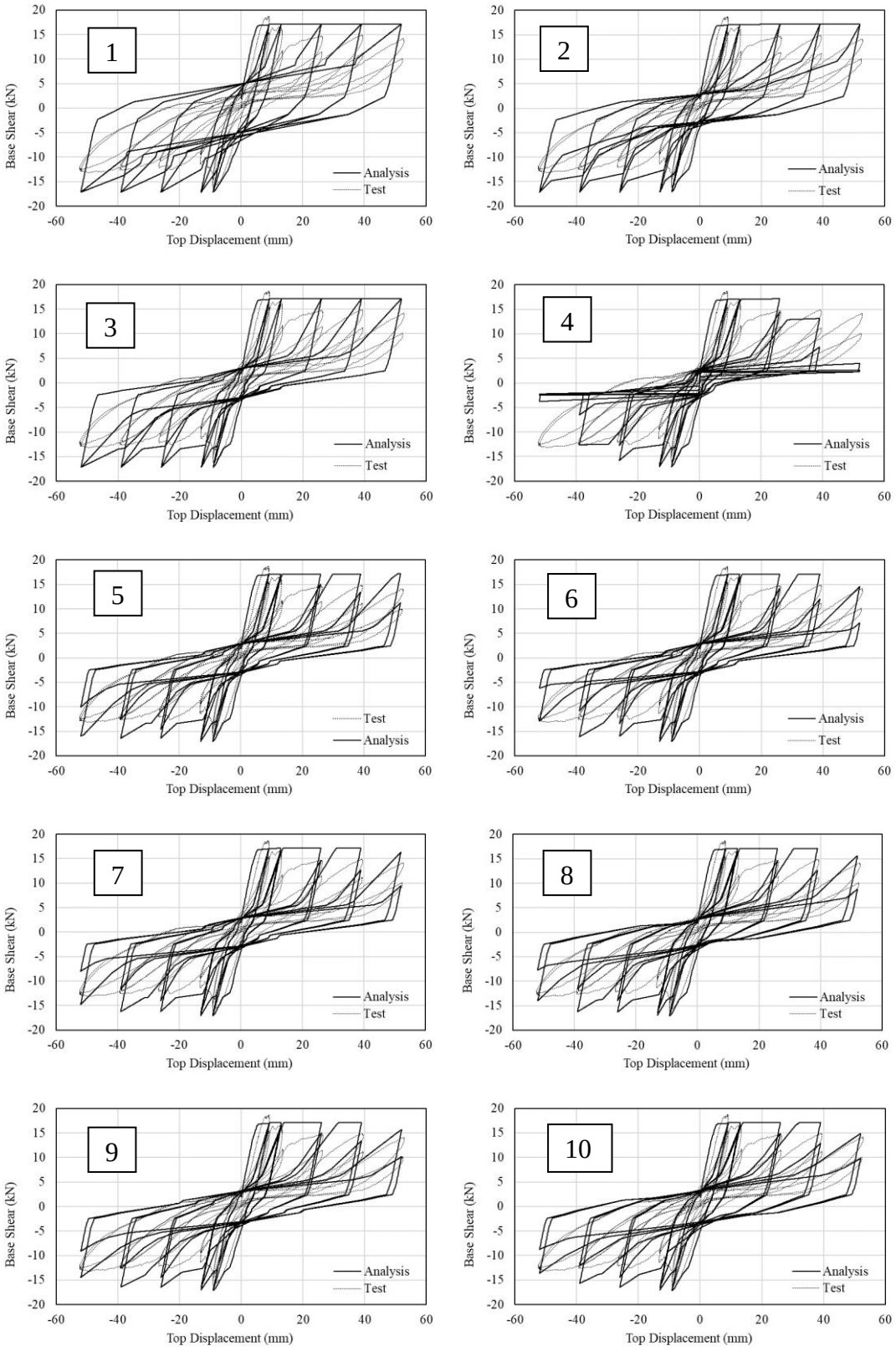

Figure 4.11: Analysis and Test Curves of Specimen PN1

4.2.1.2. Specimen PN3

Analysis and test results of the four-panel reinforced AAC panel specimen, PN3 is presented in Figure 4.12. The analysis was done for 8 different hysteretic parameter combinations. The parameters used in each graph are presented in Table 4.2. Similar to PN1, Model 1 results show the results with the default parameters of the hysteretic steel modeling without any damage. Using the experience from the analysis of PN1, *damage1* parameter was not used. The pinching parameters, *pinchx* and *pinchy* were selected as 0.5 and 0.2 to provide the best fit after observing their effects in models 2 to 5. The best-fitting model was Model 6 with the *damage2* parameter of 0.17. However, this parameter could not estimate peak strength of the response satisfactorily.

Furthermore, recognizing the recommendation of the researchers of the research program at the UT at Austin, groups of three and its permutations such as 3+3, 3+1, 3+2, 3+3+2 etc. can be modeled. For a 4-panel case, this corresponds to a 3+1 panel modeling. To see the estimation of this approach, a model was prepared with the aggregation of one-panel and three-panel analysis results. The hysteretic parameters of these models were same as the two panel approach for consistency. The result of 3 + 1 approach is presented in Figure 4.13. This approach provided better results than the four-panel monolithic approach to estimate the test behavior except the first peak capacity. The shear capacity of the test was 47.15 kN, the four-panel analysis capacity was found as 58 kN and the three plus one-panel analysis capacity was calculated as 40.18 kN. Although the first peak capacity estimations were not close to the test, three plus one-panel approach estimated the overall response satisfactorily.

Table 4.2: Hysteretic Material Parameters for Each Model in Figure 4.12

Model	*pinchx*	*pinchy*	*damage2*	Model	*pinchx*	*pinchy*	*damage2*
1	1.00	1.00	0.00	5	0.50	0.20	0.15
2	0.50	0.30	0.00	6	0.50	0.20	0.17
3	0.40	0.30	0.10	7	0.55	0.20	0.25
4	0.50	0.20	0.10	8	0.70	0.20	0.25

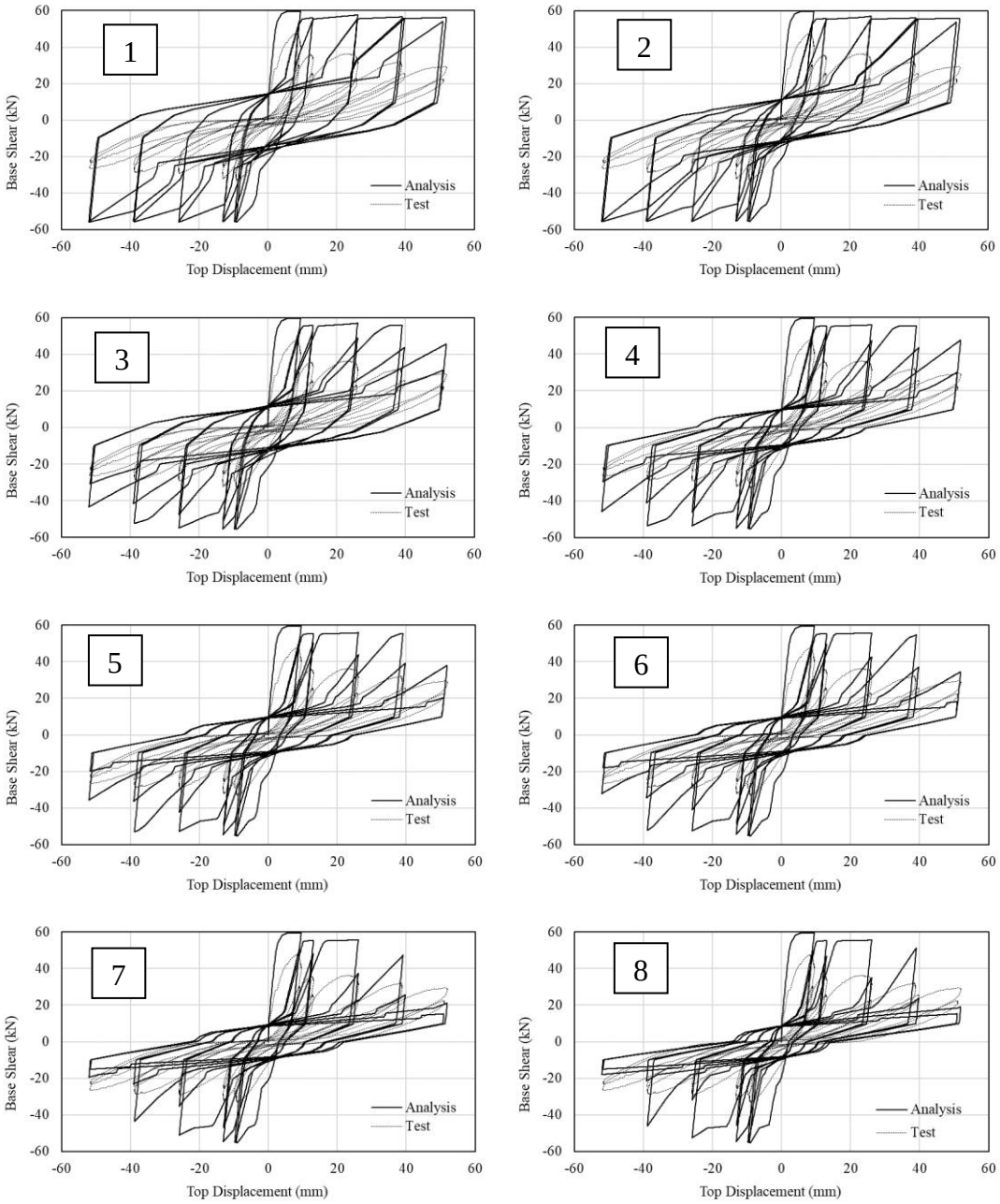

Figure 4.12: Analysis and Test Curves of Specimen PN3

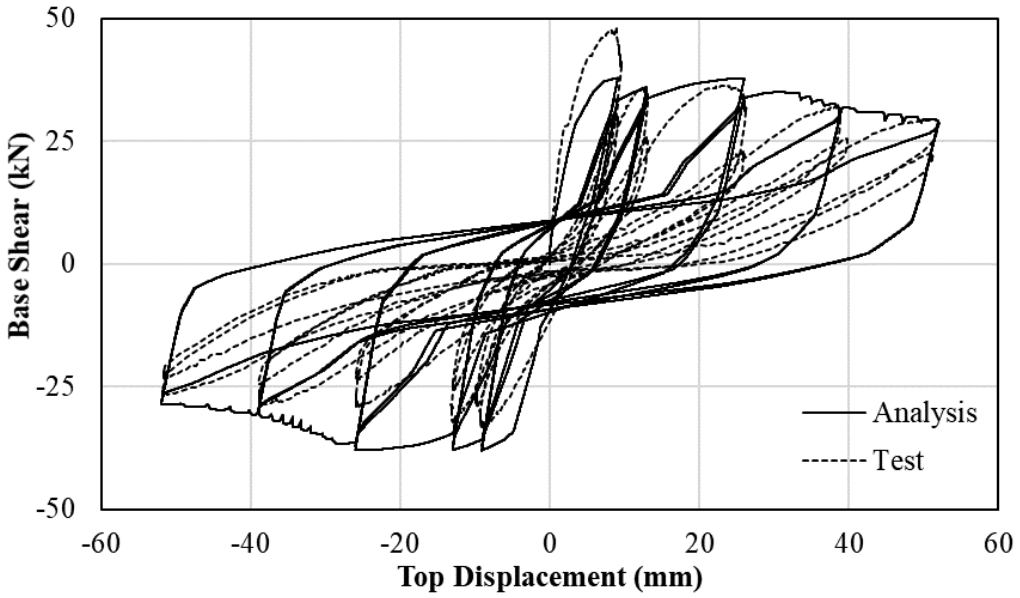

Figure 4.13: Three-Panel + One-Panel Approach vs. Test Results

4.2.1.3.Specimen PN5

In Figure 4.14, six-panel wall specimen test results and analysis results are presented. Six hysteretic parameter combinations were used in these analyses and the details are presented in Table 4.3. Model 1 results show that the default parameter analysis results estimated the test behavior satisfactorily. In order to see the effects of all hysteretic parameters, models 2 to 4 were analyzed and none of them except Model 4 estimated the real behavior of the six-panel reinforced AAC panel satisfactorily. The test shear capacity was 142.49 kN and the analysis shear capacity was 117.99 kN. These results showed that there is no systematic analysis approach to estimate the true behavior of the six-panel walls in this modeling method due to increasing irregularities with increasing number of panels. In the case of sliding shear type of failure i.e the 6 panel specimen PN5, monolithic modeling approach with default hysteretic parameters provided a satisfactory estimations.

Table 4.3: Hysteretic Material Parameters for Each Model in Figure 4.14

Model	*pinchx*	*pinchy*	*damage2*	Model	*pinchx*	*pinchy*	*damage2*
1	1.00	1.00	0.00	3	0.70	0.20	0.25
2	1.00	1.00	0.10	4	1.00	0.50	0.00

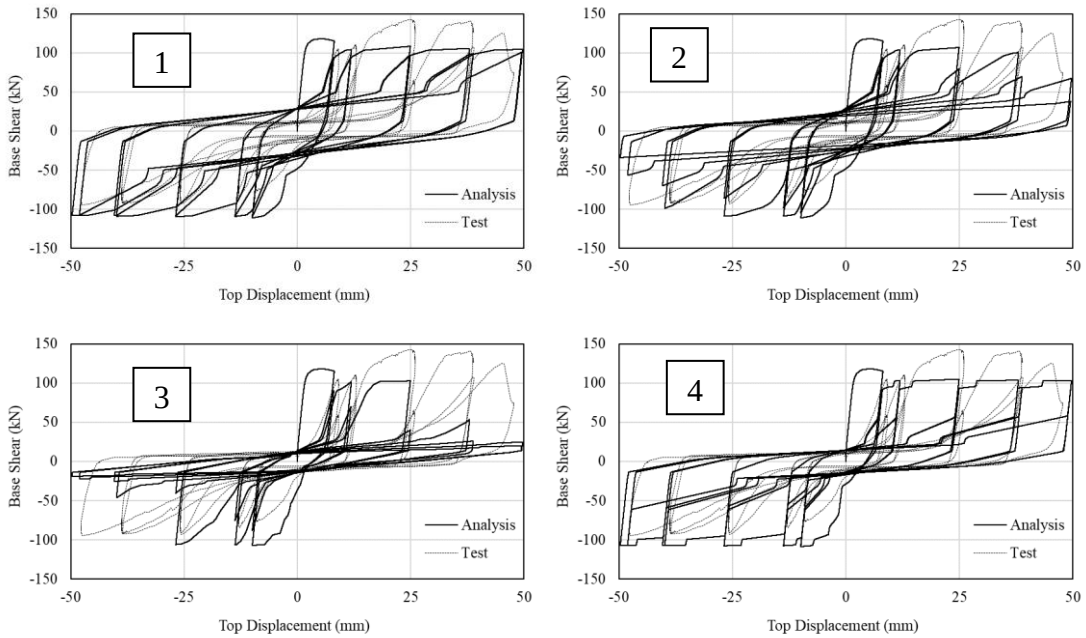

Figure 4.14: Analysis and Test Curves of Specimen PN5

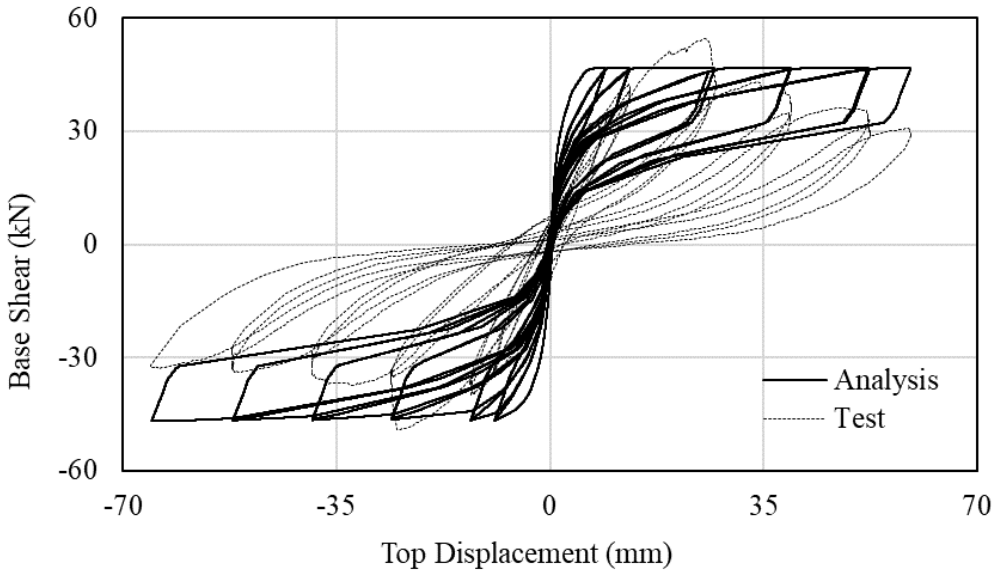

Figure 4.15: Analysis Curve for PN2 with Default Hysteretic Parameters

4.2.2. Panels with Large Axial Load Ratio {(N/N_0) > 10%}

4.2.2.1. Specimen PN2

For axial load ratios higher than %10, the panels were modeled with an elasto-plastic stress-strain model for AAC in compression in order to overcome the convergence problem. In the analysis presented in Figure 4.15, the hysteretic parameters were selected as default values. This approach estimated the capacity satisfactorily and the best estimation was obtained by *pinchx*=1.0, *pinchy*=4.0, *damage1*=0.0 and *damage2*=0.5. The pinching in the analysis was more severe than that observed in the test. Despite several analysis trials with other hysteretic parameters, a better response with the proposed fiber approach was not obtained. Hence the use of default parameters with fiber model seems to be applicable for safe estimations of energy dissipation.

4.2.2.2. Specimen PN4

In Figure 4.16, the analysis of four-panel wall and test results are presented. The analysis was first done with a four-panel model. Similar to previous wall specimen, the peak strength was not estimated satisfactorily. The test capacity was 93.68 kN and analysis capacity was calculated as 148 kN. Therefore, similar to panels with lower axial load ratio, the 3+1 panel approach was used. The 3+1 panel model with default parameters is presented in Figure 4.17. Capacity was estimated satisfactorily; however, the behavior estimation was not satisfactory. The analysis capacity is obtained as 93.3 kN. The estimation error was 0.4% and it is a quite successful estimation for shear capacity. Therefore, double two-panel approach seemed to be applicable for four-panel wall analysis similar to the four-panel wall with the axial load ratio less than 10%. Similar trials changing the hysteretic parameters, no better response estimations could be obtained.

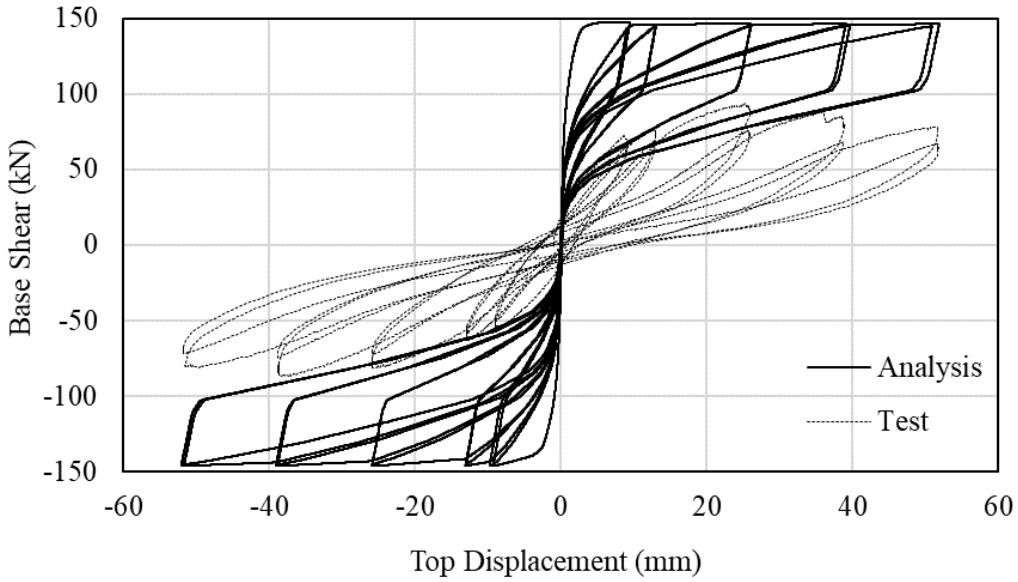

Figure 4.16: PN4 results with a section of 4 monolithic panels

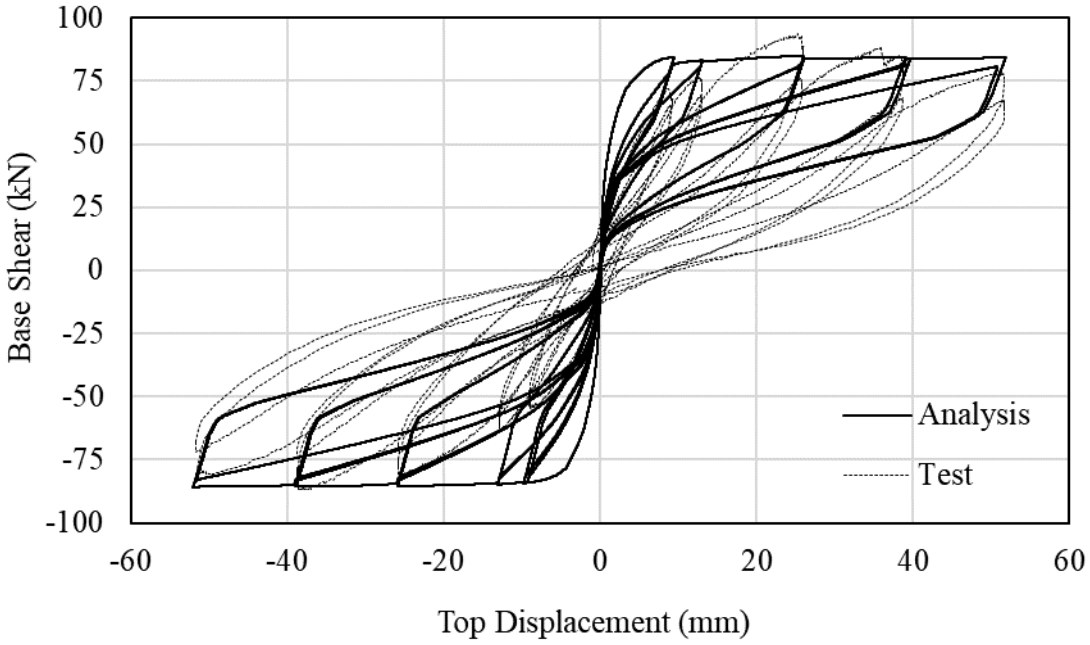

Figure 4.17: PN4 results with a 3+1 panel approach

4.2.2.3. Specimen 15a

Besides METU tests, one of the specimen, Specimen 15a, of University of Texas tests was analyzed. Since the axial load acting on the specimen was 111.7 kN, which is beyond 10 % of the axial loading capacity of the section, the specimen was modeled with elasto-plastic compressive strength material. Hysteretic parameters were default. The compressive strength of the AAC was 7.5 MPa, and the yield strength of the steel reinforcement was 520 MPa, and the ultimate strength of the steel reinforcement was 758 MPa. Monolithic wall model result is shown in Figure 4.18. The capacity and the behavior of the test specimen was estimated successfully. The test capacity was recorded as 128 kN and the analysis capacity was estimated as 123 kN. The error was 4 %. The reinforcement strength was dominant in the base shear capacity. Since there is no reinforcement between each panel except the ends the base shear capacity of these walls can be estimated monolithically.

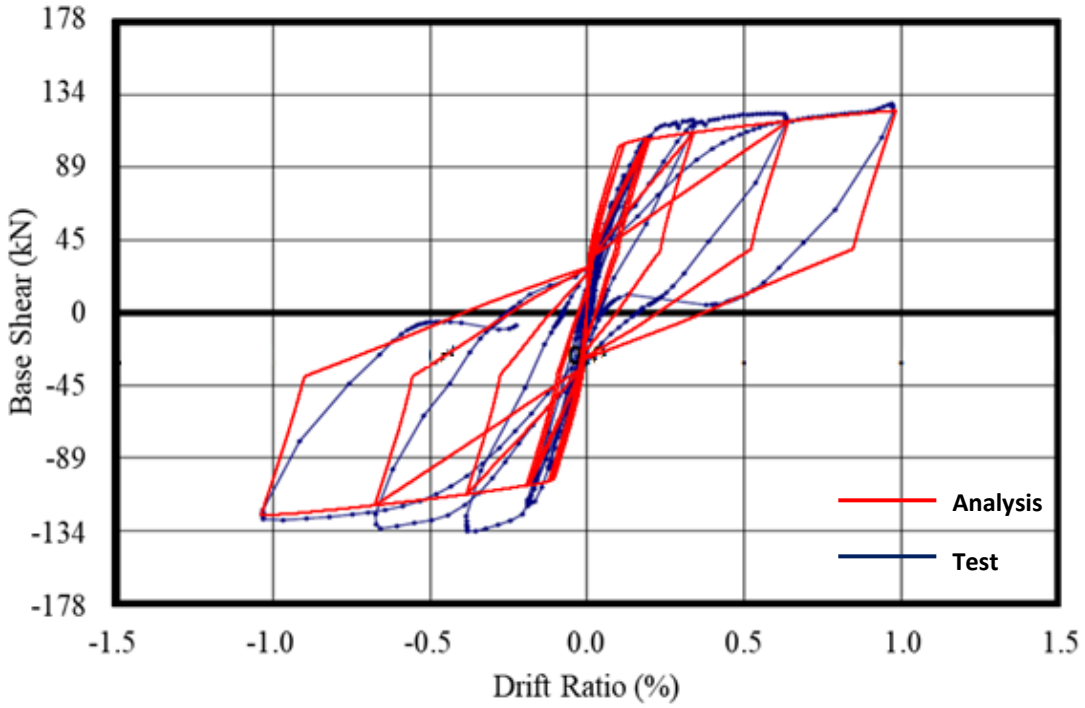

Figure 4.18: Specimen 15a results with Monolithic Panels

Modeling Recommendations

Based on the previous analysis, following steps were proposed for nonlinear modeling of reinforced AAC panel walls and buildings:

- Fiber modeling should be used by three-plus-one panels and their additions one by one without exceeding a group of three panels at once.
- AAC in compression and steel reinforcement can be modeled according to following rules:
    - For axial load ratio < 10%, a non-linear constitutive model and no tensile strength (Figure 4.1) for the AAC, and for steel models following hysteretic parameters are recommended: *pinchx*=0.7, *pinchy*=0.2 and *damage2*=0.25.
    - For axial load ratio > 10%, an elasto-plastic material model for AAC and parameters (no damage or pinching) for reinforcement is used.

4.3. Test Building Analysis

4.3.1. Modeling

Modeling of the walls of the building was conducted according to the conclusions of the previous panel simulations. Firstly, panel groups were decided according to recommendations of the researchers at UT Austin and METU. Hence selection of maximum 3 panels as a single fiber section was found appropriate. Moreover, the results of analysis of specimens PN3 and PN4 support this recommendation. Therefore, sections composed of three, two, two and a half, one and a half, and one-panels were formed. In Figure 4.19 and 4.20, the panel groups are shown. Each “wall” tag represents a panel group. Circles inside these groups are representing stick models. Since all of the walls had an axial load ratios less than of 10 %, the AAC material model was selected as a

nonlinear constitutive stress-strain response in compression. Hysteretic parameters were selected as *pinchx*=0.7, *pinchy*=0.2 and *damage2*=0.25. Beams on top of each wall were also modeled. The loading of the slabs was added to the walls according to their tributary areas. Rigid diaphragm was used in the analysis in order to satisfy the behavior of the structure. All of the modeled elements are shown in Figure 4.21. First period of the model was calculated as 0.086 s.

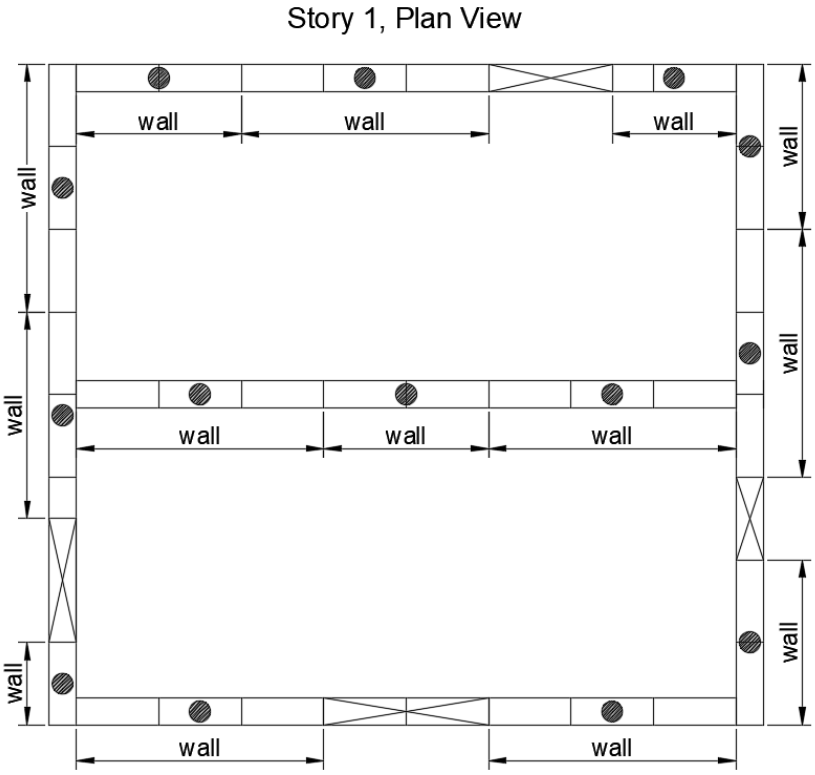

Figure 4.19: Modeling Details of First Story Walls of the Project Building

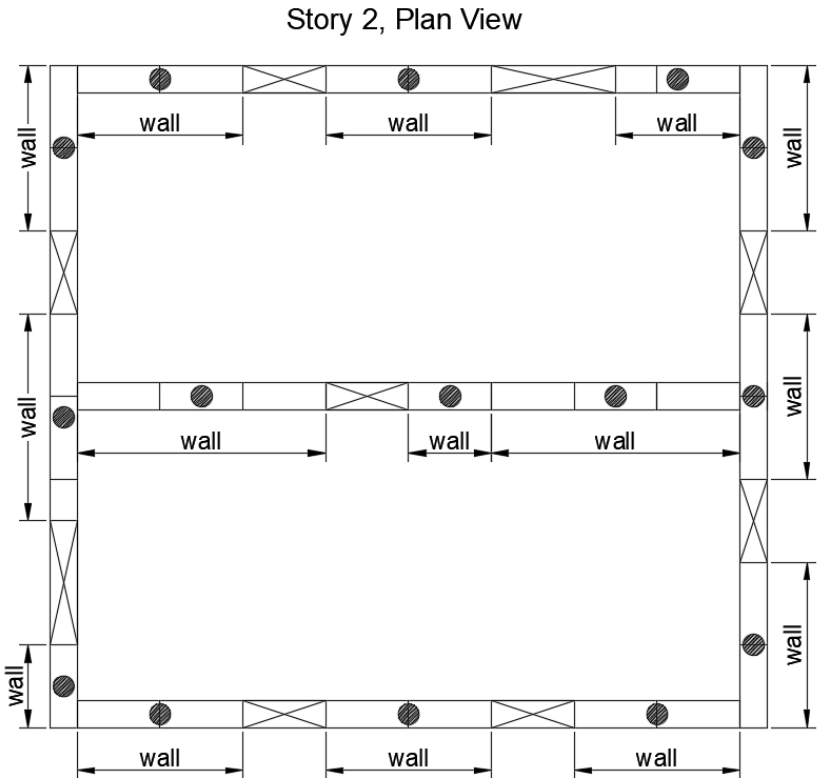

Figure 4.20: Modeling Details of Second Story Walls of the Project Building

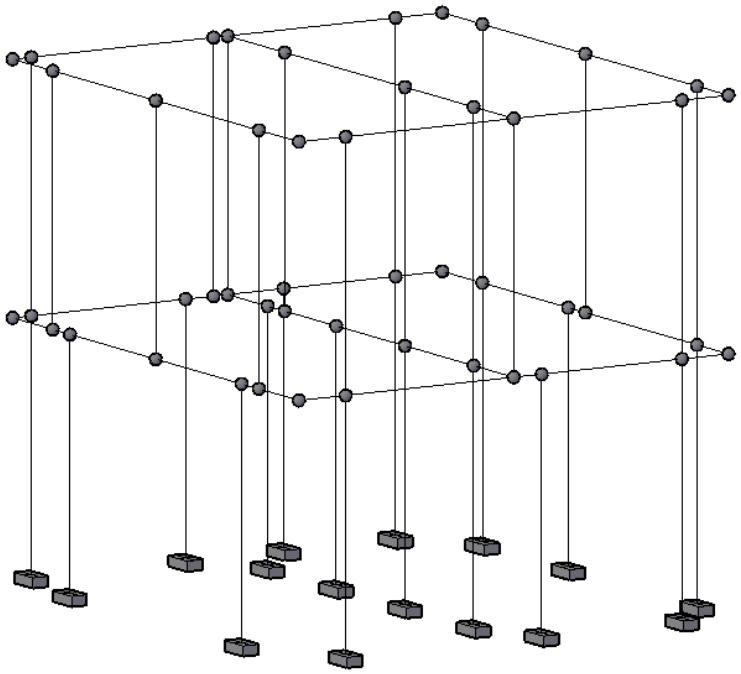

Figure 4.21: Modeling Details of the Walls of the Project Building

4.3.2. Static Analysis Results

Firstly, two static analyses were conducted before dynamic analysis. They were monolithic pushover analysis and reversed cyclic pushover analysis. The pushover analysis result is presented in Figure 4.22. The lateral load capacity was estimated as 591.3 kN and the test capacity was 580 kN (-605 kN). In the test, this capacity was recorded at 11 mm top displacement, and in the analysis, it was 17 mm. Then, the pushover capacity curve decreased to a capacity of 488.5 kN whereas the test capacity decreased to 311 kN (-302 kN) in the last cycle. The cyclic pushover analysis result are shown in Figure 4.23. Although the capacity was achieved in the cyclic analysis similar to pushover analysis, the descending branch was not obtained satisfactorily due to complications such as combination of as rocking and sliding of the walls in addition crushing of the toes and buckling of the steel reinforcements. These deformations significantly decreased the capacity after the peak capacity was achieved in the test. However, simulations did not include those phenomena.

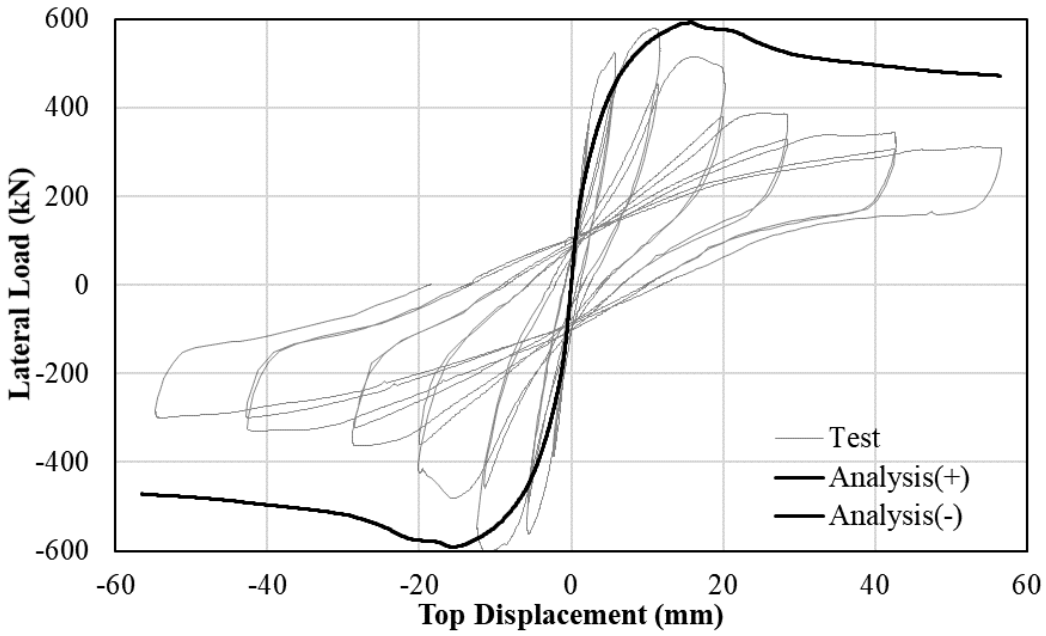

Figure 4.22: Pushover Analysis Result of the Building Model

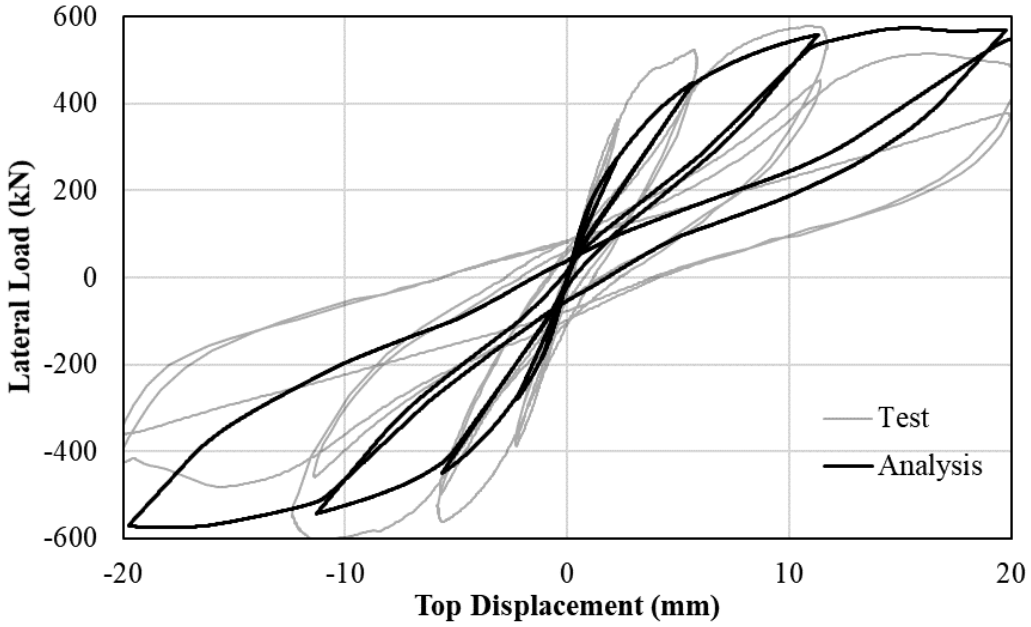

Figure 4.23: Cyclic Pushover Analysis Result of the Building Model

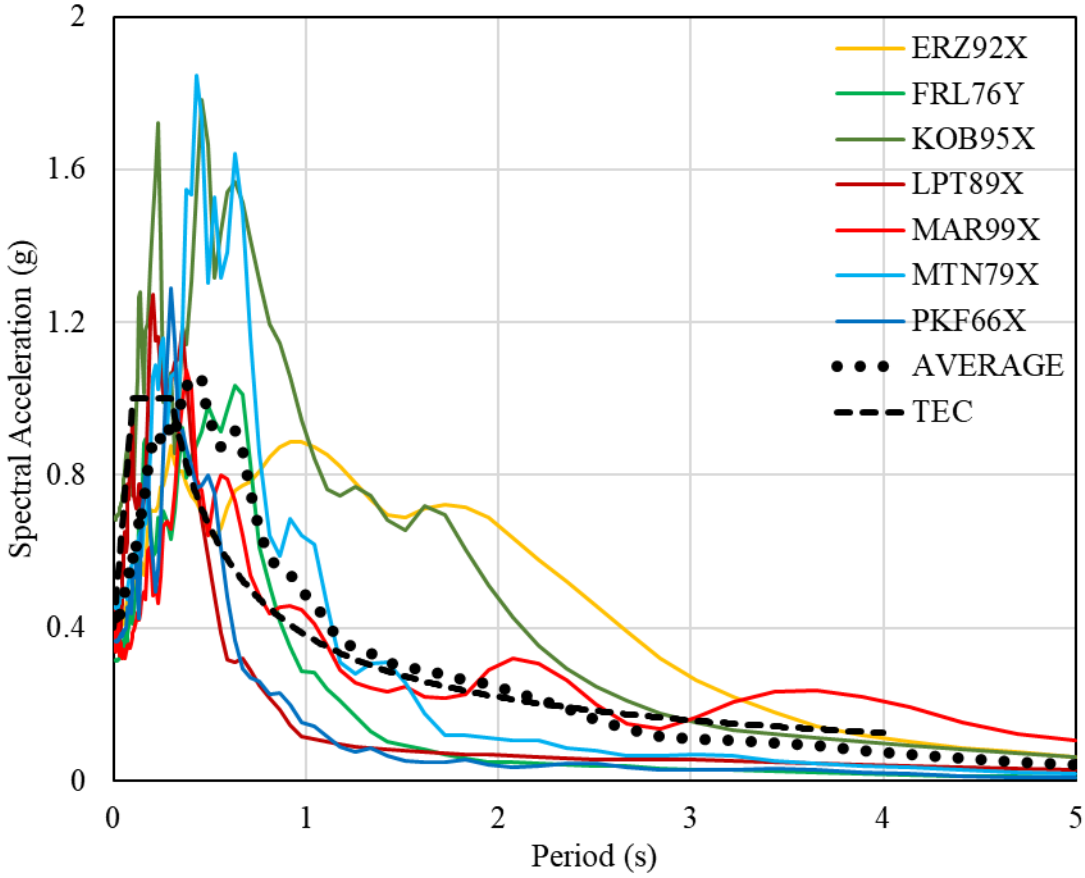

Figure 4.24: Spectral Acceleration vs. Period of Seven Earthquakes

4.3.3. Dynamic Analysis Results

Seven different earthquakes, their details are shown in Figure 4.24 and Table 4.4, were used for the dynamic analysis by ground acceleration scaling. Incremental dynamic analyses was applied to the building model using these earthquake data. From Figure 4.25 to Figure 4.28, incremental dynamic results are presented. Up to 1.0g, the building model stayed in the elastic region and maximum interstory drift ratio was observed 0.054 %. At 1.5g ground acceleration, the base shear capacity was reached and the drift ratio was 0.11 %. After 1.5g, the models started go beyond capacity and first signs of collapse were observed.

After the incremental dynamic analyses were finished, maximum interstory drift ratio of each earthquake analyses were plotted with respect to ground acceleration scales in Figure 4.29, which is the summary of the all analyses. As a result, this plot shows that the collapse was between 1.7g and 2.2g with 0.2 - 0.3 % maximum interstory drift ratio. This result approves the findings of METU Building Test. Building analyses show that AAC building are expected to behave mostly in their elastic state. Under severe events, some deforming capacity is available. The maximum interstory drift ratio of the AAC buildings should be limited to about 0.3 % to achieve collapse prevention during design.

Table 4.4: Details of the Earthquakes Used in the Incremental Dynamic Analysis

No	ECODE	Earthquake	Country	Date	Location	F. Type	Interval	PGA (g)
1	PKF66X01	Parkfield	USA	28.06.1966	Cholame #5	Rt Lat Strike Slip	0.01	0.367
2	FRL76Y01	Friuli	Italy	06.05.1976	Tolmezzo, Diga Ambiesta	Thrust	0.01	0.316
3	MTN79X01	Montenegro	Form. Yugoslavia	15.04.1979	Petrovac, Hotel Oliva	Thrust	0.01	0.454
4	LPT89X04	Loma Prieta	USA	18.10.1989	Gilroy Array #1	Oblique	0.02	0.435
5	ERZ92X01	Erzincan	Turkey	13.03.1992	Erzincan	Strike Slip	0.01	0.389
6	KOB95X03	Kobe	Japan	16.01.1995	Takarazu	_	0.01	0.693
7	MAR99X04	Marmara	Turkey	17.08.1999	Düzce	Strike Slip	0.005	0.337

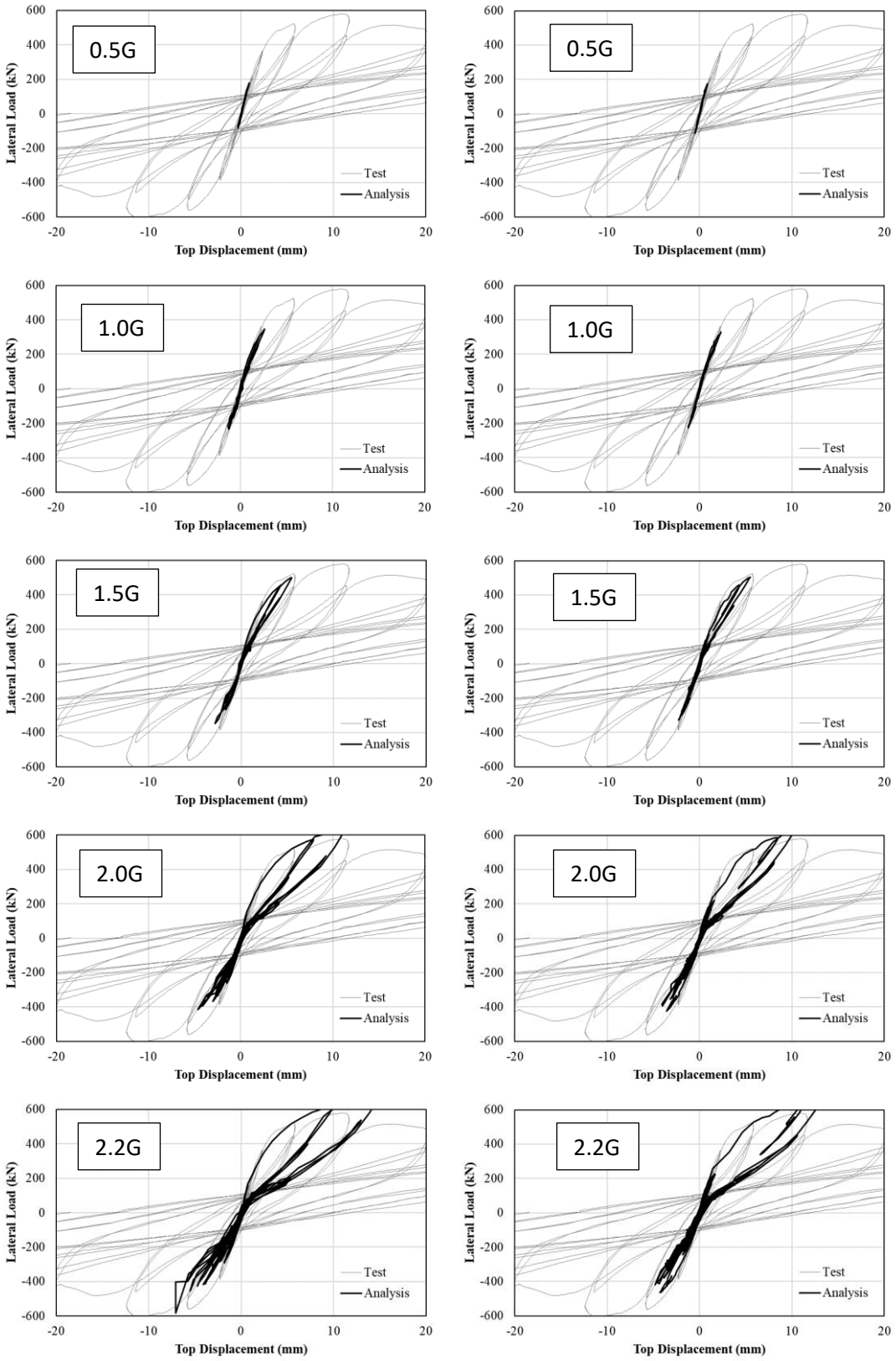

Figure 4.25: Results of KOB95X (Left Column) and ERZ92X (Right Column)

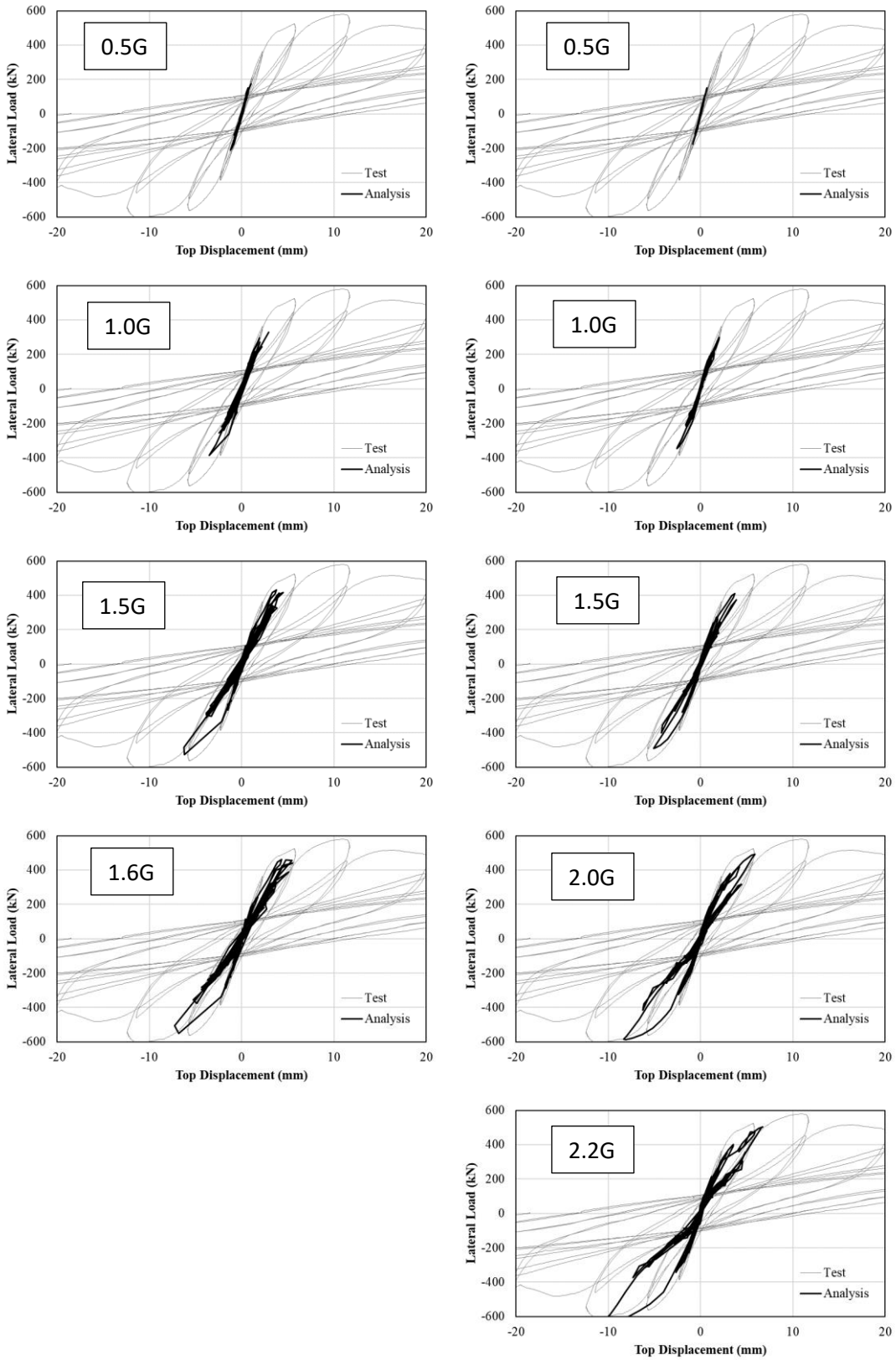

Figure 4.26: Results of LPT89X (Left Column) and PKF66X (Right Column)

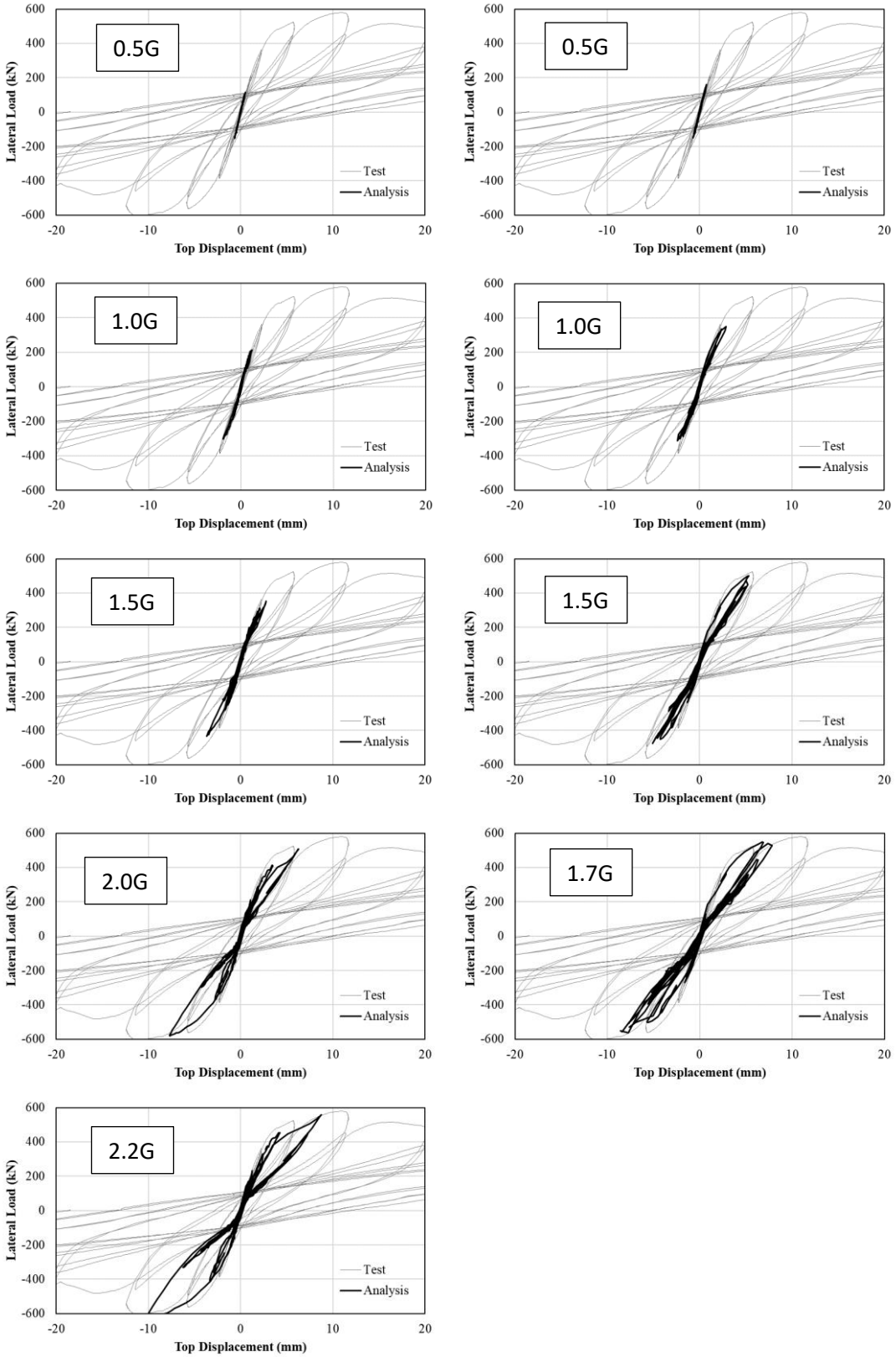

Figure 4.27: Results of MAR99X (Left Column) and FRL76Y (Right Column)

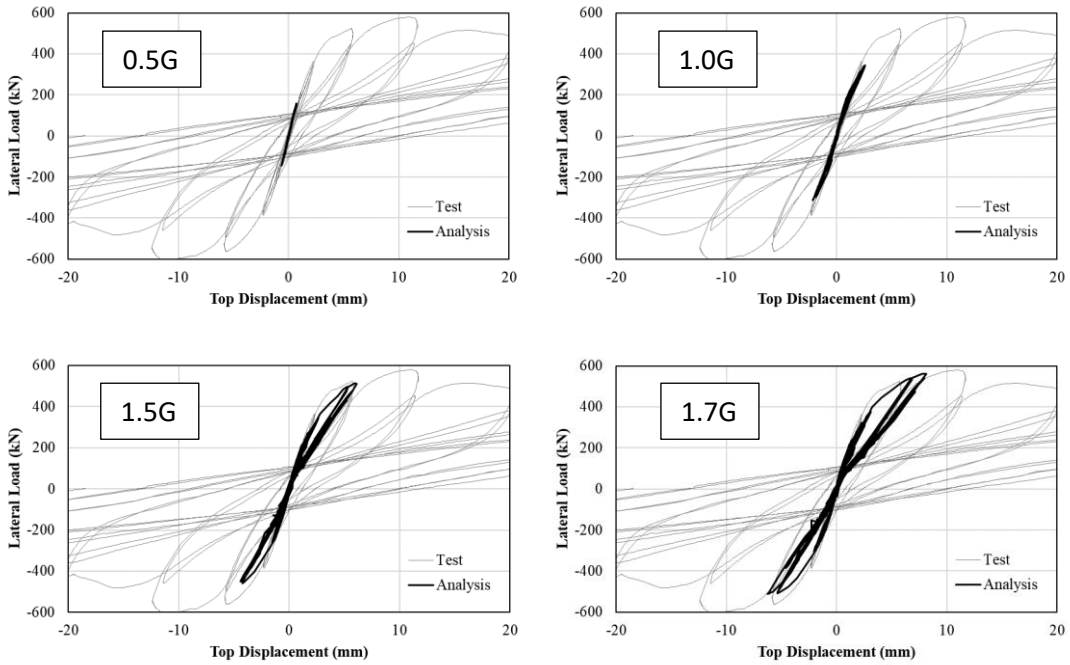

Figure 4.28: Result of MTN79X

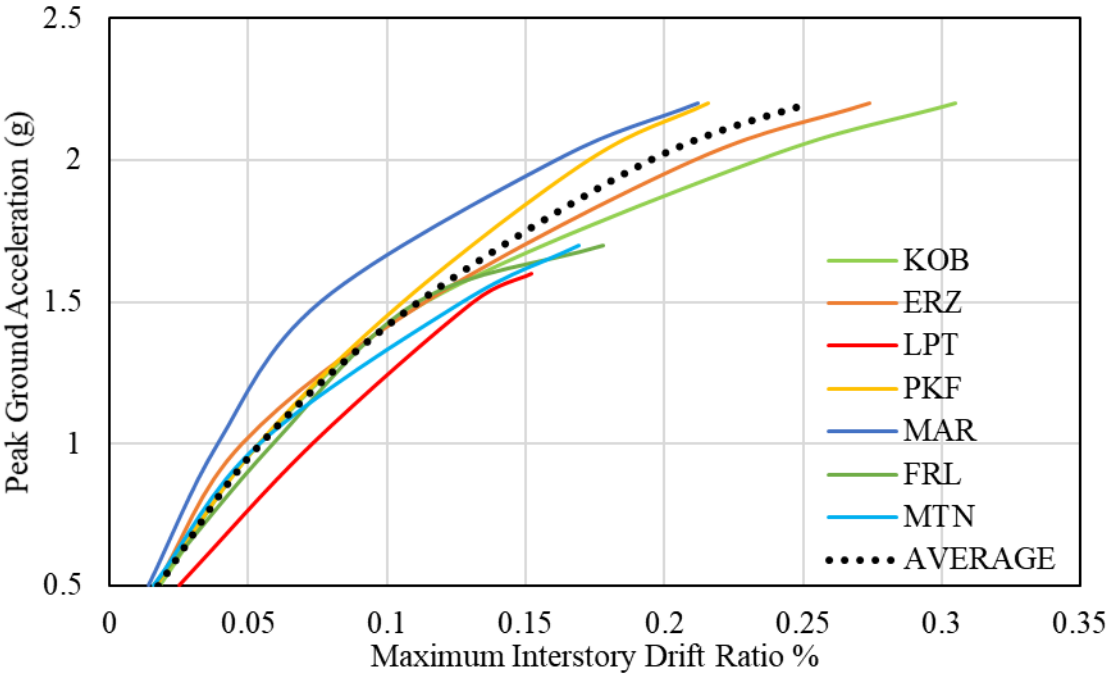

Figure 4.29: Peak Ground Acceleration vs Maximum Interstory Drift Ratio Results of Incremental Dynamic Analysis of Seven Earthquakes

CHAPTER 5

CONCLUSION

5.1. Summary

Computational models of reinforced AAC panel walls and buildings were analyzed in this study. The models were calibrated with tests performed previously on the reinforced AAC panel walls. Then, the results were compared with earlier studies carried out at the UT Austin and METU to develop a design and analysis methodology for reinforced AAC panel walls and buildings in Turkey. Firstly, shear wall specimens of METU project were modeled. AAC and steel reinforcement material are modeled using fiber sections, which were utilized in nonlinear force based beam column frame elements. Then, these elements under constant axial loading were laterally loaded cyclically with a displacement-controlled approach using experimental data of METU project. Secondly, the two-story reinforced AAC panel building was analyzed with static and incremental dynamic analysis using the models developed in the first part of the study. According to recommendations of previous works and simulations performed in this study, the walls were separated to groups of maximum three panels. Then, the reinforced concrete beams were modeled with the panel elements. Rigid diaphragm approximation was also used.

5.2. Conclusions

The following conclusions were drawn from these analyses:

- The walls with their axial load ratio (N/N_0) above %10 and below %10 should be modeled with different approaches.
- Below %10 of (N/N_0), the AAC material can be represented with its realistic behavior. Moreover, steel reinforcement hysteretic parameters, pinching and damage parameters should be calibrated accordingly.
- Above %10 of (N/N_0), the AAC material must be modeled with elastic-plastic material model due to severe convergence problems. Furthermore, hysteretic parameters can stay default.
- 4-panel walls can be modeled by 3+1 panel walls. The capacity results fit with each other for both above and below of axial load ratio of %10.
- Panel walls expected to experience sliding shear failures should be modeled as monolithic walls
- From the tests, 2-panel walls show flexural failure, 4-panel walls undergoe flexural-shear failure and 6-panel walls fail due to sliding shear. Therefore, the design equations should apply according to the aspect ratio of the wall.
- AAC buildings, due to their lightweight nature, are expected to behave in their pre-yielding regions under design earthquakes.
- Under extreme events, there seems to exist some deformation and energy dissipation capacity which can help AAC buildings to swing without collapse.
- Based on these results AAC buildings appear to be a good alternative for low rise construction in seismic regions.

REFERENCES

Aircrete Europe. (n.d.). *What is Autoclaved Aerated Concrete (AAC)?* Retrieved August 14, 2017, from http://www.aircrete-europe.com/en/aircrete-aac/what-is-autoclaved-aerated-concrete.html

Argudo, J. F. (2003). *Evaluation and Synthesis of Experimental Data for Autoclaved Aerated Concrete*. PhD thesis, The University of Texas at Austin.

Balkema, A. A. (1992). *Advances in autoclaved aerated concrete*. F. H. Wittmann (Ed.). AA Balkema.

Boggelen, W. V. (2014). *History of Autoclaved Aerated Concrete: The Short Story of a Long Lasting Building Material*. Aircrete-Europe

European Committee for Standardization, Brussels, Belgium. *Eurocode 6 - Design of masonry structures*, 2005.

European Committee for Standardization, Brussels, Belgium. *Eurocode 8: Design of structures for earthquake resistance,* 2004.

European Committee for Standardization, Brussels, Belgium. *Prefabricated Reinforced Components of Autoclaved Aerated Concrete*, 2015.

Imber, M. G. (n.d.). *Casa De Las Lomas*. Retrieved September 12, 2017, from https://www.michaelgimber.com/projects/casa-de-las-lomas/

Abramowitz, M. & Stegun, C. A. (1972). *Handbook of Mathematical Functions with-Formulas, Graphs, and Mathematical Tables*. Dover, New York, NY, USA.

MSJC (2011). *Building Code Requirements for Masonry Structures* (MSJC).

Myanmar Business (2017) *Amazing Benefits Of AAC Blocks*. Retrieved August 16, 2017, from https://myanmarbusinessinfo.blogspot.com.tr/2017/01/amazing-benefits-of-aac-blocks.html

OpenSees (n.d.) *OpenSees Command Manual*. Retrieved from http://opensees.berkeley.edu/wiki/index.php/Command_Manual

Ozel, M. (2011). Thermal performance and optimum insulation thickness of building walls with different structure materials. *Applied Thermal Engineering*, 31(17-18), 3854-3863

Schnitzler, S. (2006). *Applied Research Paper: Autoclaved Aerated Concrete as a Green Building Material*. Sustainability and the Built Environment UC Davis Extension

Taghipour, A. (2016). *Seismic Behavior of Vertical Reinforced Autoclaved Aerated Concrete (AAC) Panel Walls*. MS Thesis, Middle East Technical University.

Tanner, J., Varela, J., Brightman, M., Cancino, U., Argudo, J., and Klingner, R. (2005). Seismic Testing of Autoclaved Aerated Concrete Shearwalls: A Comprehensive Review. *ACI Structural Journal,* 102(3), 374-382.

Tanner, J. E. (2003). *Design provisions for Autoclaved Aerated Concrete (AAC) structural systems*. PhD thesis, The University of Texas at Austin.

TEC (2016). *Turkish Earthquake Code 2016*.

Varela, J. L. (2003). *Development of R and Cd factors for the seismic design of AAC structures*. PhD thesis, The University of Texas at Austin.

Xella Aircrete North America, Inc. (2010). *Technical Manual*. Retrieved August 14, 2017, from http://www.hebel-usa.com/en/content/technical_manual_1795.php

YTONG. (n.d.). Load Bearing Vertical Wall Elements. Retrieved August 28, 2017, from http://ytong.com.tr/urunler_db.asp?urunID=20